

2023-08-05

A storm driven turbidity maximum in a microtidal estuary

Postacchini, M

<https://pearl.plymouth.ac.uk/handle/10026.1/21017>

10.1016/j.ecss.2023.108350

Estuarine, Coastal and Shelf Science

Elsevier

All content in PEARL is protected by copyright law. Author manuscripts are made available in accordance with publisher policies. Please cite only the published version using the details provided on the item record or document. In the absence of an open licence (e.g. Creative Commons), permissions for further reuse of content should be sought from the publisher or author.

Estuarine, Coastal and Shelf Science

A Storm Driven Turbidity Maximum in a Microtidal Estuary

--Manuscript Draft--

| | |
|------------------------------|--|
| Manuscript Number: | YECSS-D-22-00586R2 |
| Article Type: | Research Paper |
| Keywords: | microtidal estuary; wave-current interaction; Turbidity Maxima Zone; flocc dynamics; estuarine dynamics |
| Corresponding Author: | Matteo Postacchini Universita Politecnica delle Marche Ancona, Ancona ITALY |
| First Author: | Matteo Postacchini |
| Order of Authors: | Matteo Postacchini Andrew J. Manning Joseph Calantoni Joseph P. Smith Maurizio Brocchini |
| Abstract: | <p>Many macro- and mesotidal estuaries are characterized by Turbidity Maxima Zones (TMZs), regions with suspended solid concentrations that are much higher than those found throughout the rest of the estuary. Such regions are located near the upriver limit of salt intrusion and their position and extent are modulated and driven by tidal oscillations, especially in estuaries where tidal forcing is large. Hence, pronounced TMZs are not typically expected in micro-tidal estuaries. Field experiments were carried out in the microtidal estuary of the Misa River (northeast coast of Italy) with the aim to analyze riverine-coastal ocean interactions during different climatic conditions, freshwater discharge and tidal forcing. The goal was also that of identifying factors and episodic conditions that could lead to the evolution of ephemeral TMZs in this microtidal estuarine system. Observational results, combined to a flocculation model suite, describe the hydrodynamics, morphological bed evolution, water chemistry and flocc dynamics within the estuary during wintertime quiescent and stormy periods. Pronounced TMZs with different location and extent were observed during two storms with different intensities, when enhanced freshwater discharge, wave action and tidal oscillation generated significant stratification of the lower estuarine water column. Higher turbidity values were observed throughout the TMZ during the smaller/weaker storm, while stronger surface mixing during the stronger storm led to greater dispersion of the (re-)suspended particulate load throughout the upper water column, providing a less pronounced TMZ along the bed of the lower estuary. Observations in the Misa River, potentially valid for other microtidal estuaries, show that: 1) episodic storm conditions that significantly increase freshwater discharge can lead to the evolution of an ephemeral TMZ that is modulated, but not controlled, by tidal oscillations and surface mixing conditions; 2) ephemeral TMZ localization, intensity, and extent during episodic storm events is a function of storm intensity; 3) moderately enhanced freshwater flow during an episodic storm event promotes a high degree of stratification, allowing for the formation of large flocs with great settling rates, leading to a pronounced TMZ forming downriver of the landward limit of seawater intrusion; whereas higher freshwater flows during stronger storm events lead to less stratification, greater bottom turbulence and potential TMZ suppression near the riverbed, with shear conditions promoting smaller flocs with lower settling and a greater potential for suspended particulate export from the lower estuary to coastal waters.</p> |
| Suggested Reviewers: | <p>Tian-Jian Hsu thsu@udel.edu</p> <p>Claire Chassagne c.chassagne@tudelft.nl</p> <p>Courtney K. Harris ckharris@vims.edu</p> |

| | |
|-------------------------------|--|
| | David H. Schoellhamer dschoell@usgs.gov |
| Opposed Reviewers: | |
| Response to Reviewers: | |

Dear Editor,

I am pleased to re-submit the revised version of the article

“A Storm Driven Turbidity Maximum in a Microtidal Estuary”

by Matteo Postacchini, Andrew J. Manning, Joseph Calantoni, Joseph Smith & Maurizio Brocchini.

Following the constructive comments from Reviewer #2, we have improved the manuscript, which is now significantly shorter than the previous versions, as many parts have been condensed or rearranged. The other suggestions have also been addressed, especially concerning the estimate of the shear stress and the improvement of some sentences.

The manuscript has not been published and is not under consideration for publication elsewhere. We have no conflicts of interest to disclose.

In view of the above listed points, we hope that the present version could be suitable for publication.

Sincerely,

Matteo Postacchini

Reviewer #2

We thank the Reviewer for her/his comments and suggestions. We have thoroughly revised the manuscript (new text in red), and a point-by-point reply is provided here below.

The paper would be much clearer if it were condensed and focused on the main points summarized in the conclusion. The section on floc settling and the floc model are ancillary to the main points in the paper.

The paper is greatly improved, but still would benefit by being more concise. Still, there is a lot of data and results that might be relevant to other studies, and so I would not reject it from publication just for excessive wordiness.

The manuscript has been shortened, following Reviewer's suggestions. Some ancillary parts have been removed, as we understand that some sections may be reduced to make the paper concise and more readable for the audience (e.g., see sections 1, 2.3, 4). Furthermore, fig.3 has been modified removing the original panels b, which illustrated local wind and precipitation. In the end, the main portion of the paper (i.e. up to the Conclusion section) has been shortened of more than 60 lines. Some of the appendices have also been removed.

Other parts (apparently of less importance) have been retained because of their role in the TMZ dynamics. As an example, the flocculation part is relevant within the analysis of the TMZ in our MTE, especially for the influence that such phenomenon might have on, e.g., the pollutant transport, sedimentary residence time, contaminant retention. Section 2.3 has been thus kept, although it is now shorter.

line 579, I think using the local longitudinal slope is probably not appropriate in a tidal estuary. I suspect the variable i is based on estimating the surface slope of the water using the slope of the bed, which would work in a freshwater channel. But here the slope varies with the tide, in fact, creating surface slopes and currents that go into the estuary, not out. Nevertheless, the method includes the velocity shear and should provide a good qualitative measure of the shear stress?

Following Reviewer's suggestion, we have recalculated the shear velocity based on the classic logarithmic profile. This led to a shear stress much smaller than that originally calculated, thus leading to a result that better fits the flocculation model hypotheses (see new figure 8 and lines 529-537).

line 623 It's not clear why the lower water surface elevation would facilitate wave propagation. The lower water would make waves break more which would reduce propagation and lower water would also create more friction felt by the waves which would further dampen their propagation.

We agree that the sentence was not clear enough, as we were referring to the lower river discharge and non-breaking waves penetrating the estuary. It has been amended and now reads (from line 576): "However, the lower river flow (during the ebb tide, at low tide and in the beginning of the flood tide) facilitated the propagation of low-energy/non-breaking waves into the estuary, thus leading to a strong interaction between river forcing and waves at the mouth, which affected both gravitational circulation and TMZ generation."

line 643 "well stratified structure in the final reach of the river" but in the next sentence the authors state that the water was more stratified upriver and less stratified at the mouth. Are the authors considering the upriver section to be the "final reach". If so, I think this would confuse most people.

We agree with the Reviewer. The sentence has been modified, specifying that the well-stratified structure occurred at a distance of 300 to 600 m from the mouth (line 596).

line 675 "high shear stress ... which was induced by the intense flow, rather than by an almost negligible vertical shear" There must be shear for shear stress to be created. The vertical shear is probably closer to the bed in this situation rather than higher in the water column.

The sentence was misleading. It has been amended and now underlines the high values of both eddy viscosity and shear velocity (see equations 4 and 5) compared to the pure velocity shear dV/dz (line 628).

line 701 a lot of this information in 4.1 is redundant with the previous section. It should be condensed or merged with the previous section 4.

Section 4.1 is now merged to section 4. We took advantage of compacting the whole current section 4.

- Observations of Turbidity Maxima Zone (TMZ) and modeling of floc dynamics
- TMZ observed during two storms occurred at the microtidal Misa River estuary, Italy
- TMZ evolving along the river during storms, the tide only modulating the flow
- High stratification during moderate-flow conditions: more likely TMZ formation
- Large mixing and reduced flocculation during high-flow conditions: TMZ suppression

Declaration of interests

The authors declare that they have no known competing financial interests or personal relationships that could have appeared to influence the work reported in this paper.

The authors declare the following financial interests/personal relationships which may be considered as potential competing interests:

Maurizio Brocchini reports financial support was provided by Office of Naval Research Global. Maurizio Brocchini reports financial support was provided by Government of Italy Ministry of Education University and Research. Andrew J. Manning reports financial support was provided by US National Science Foundation. Joseph Calantoni reports financial support was provided by Office of Naval Research. Maurizio Brocchini reports a relationship with Gestiport spa that includes: consulting or advisory.



Click here to access/download
Supplementary Material
TMZ_ecss_R2_v2_marked.docx



Author Statement

M. Postacchini, Andrew J. Manning, Joseph Calantoni, Joseph P. Smith, Maurizio Brocchini

Conceptualization: MP AJM JC JPS MB

Methodology: MP AJM JC MB

Formal analysis: MP AJM JC JPS

Investigation: MP AJM JC JPS MB

Resources: MP AJM JC JPS MB

Data curation: MP JC JPS

Writing—original draft preparation: MP AJM

Writing—review and editing: MP AJM JC JPS MB

Visualization: MP JC JPS

Supervision: JC MB

Project administration: MP JC JPS MB

Funding acquisition: AJM JC MB

A Storm Driven Turbidity Maximum in a Microtidal Estuary

M. Postacchini¹, Andrew J. Manning^{2,3,4,5,6}, Joseph Calantoni⁷, Joseph P. Smith⁸, Maurizio Brocchini^{1,4,9}

¹Università Politecnica delle Marche, Ancona, Italy.

²HR Wallingford, Coasts and Oceans Group, Wallingford, UK.

³Environment and Energy Institute, University of Hull, Hull, UK.

⁴University of Florida, Gainesville, FL, USA.

⁵Stanford University, Stanford, California, USA.

⁶University of Plymouth, Plymouth, Devon, UK.

⁷Ocean Sciences Division, U.S. Naval Research Laboratory, Stennis Space Center, MS, USA.

⁸Department of Ocean and Atmospheric Sciences, U. S. Naval Academy, Annapolis, MD, USA.

⁹CoNISMa ULR Ancona, Ancona, Italy.

Corresponding author: Matteo Postacchini (m.postacchini@staff.univpm.it)

Abstract

Many macro- and mesotidal estuaries are characterized by Turbidity Maxima Zones (TMZs), regions with suspended solid concentrations that are much higher than those found throughout the rest of the estuary. Such regions are located near the upriver limit of salt intrusion and their position and extent are modulated and driven by tidal oscillations, especially in estuaries where tidal forcing is large. Hence, pronounced TMZs are not typically expected in micro-tidal estuaries. Field experiments were carried out in the microtidal estuary of the Misa River (northeast coast of Italy) with the aim to analyze riverine-coastal ocean interactions during different climatic conditions, freshwater discharge and tidal forcing. The goal was also that of identifying factors and episodic conditions that could lead to the evolution of ephemeral TMZs in this microtidal estuarine system. Observational results, combined to a flocculation model suite, describe the hydrodynamics, morphological bed evolution, water chemistry and floc dynamics within the estuary during wintertime quiescent and stormy periods. Pronounced TMZs with different location and extent were observed during two storms with different intensities, when enhanced freshwater discharge, wave action and tidal oscillation generated significant stratification of the lower estuarine water column. Higher turbidity values were observed throughout the TMZ during the smaller/weaker storm, while stronger surface mixing during the stronger storm led to greater dispersion of the (re-)suspended particulate load throughout the upper water column, providing a less pronounced TMZ along the bed of the lower estuary. Observations in the Misa River, potentially valid for other microtidal estuaries, show that: 1) episodic storm conditions that significantly increase freshwater discharge can lead to the evolution of an ephemeral TMZ that is modulated, but not controlled, by tidal oscillations and surface mixing conditions; 2) ephemeral TMZ localization, intensity, and

38 extent during episodic storm events is a function of storm intensity; 3) moderately enhanced
39 freshwater flow during an episodic storm event promotes a high degree of stratification, allowing
40 for the formation of large flocs with great settling rates, leading to a pronounced TMZ forming
41 downriver of the landward limit of seawater intrusion; whereas higher freshwater flows during
42 stronger storm events lead to less stratification, greater bottom turbulence and potential TMZ
43 suppression near the riverbed, with shear conditions promoting smaller flocs with lower settling
44 and a greater potential for suspended particulate export from the lower estuary to coastal waters.

45 **Keywords:** microtidal estuary; wave–current interaction; Turbidity Maxima Zone; floc dynamics;
46 estuarine dynamics

47

48 **1 Introduction**

49 To improve the management and maximize the resilience of coastal systems, an increase
50 in the understanding of estuarine processes, including the hydrodynamics and sediment transport
51 in estuaries, is needed (Bertin & Olabarrieta, 2016; Melito et al., 2018). Estuarine processes differ
52 between different estuary types, which can be defined by many factors such as geomorphology,
53 tidal range, and mixing (Davies, 1964; Cooper, 2001). Furthermore, estuarine dynamics and
54 circulation depends on the complex interplay between tides, wind waves, freshwater outflow,
55 sediment transport and accumulation, and geomorphology. Full understanding of estuarine
56 dynamics and circulation is still a challenge (Anthony, 2015; Bertin & Olabarrieta, 2016;
57 Brocchini 2020). Additional complexity derives from the active mixing between freshwater
58 inflows and ocean water, leading to differing degrees of stratification and mixing, and strong
59 spatial and temporal variations of physiochemical and chemical parameters such as turbidity,
60 nutrient concentrations, salinity, temperature, pH, and dissolved oxygen that can in turn influence
61 biological productivity (Pritchard, 1967; Talke et al., 2009; Geyer & MacCready, 2014).

62 Estuaries are often categorized as micro-, meso- and macrotidal estuaries (Davies, 1964).
63 Microtidal estuaries (absolute tidal range < 2 m and relative tidal range < 3) are dominated by
64 wind, wave forcing and freshwater inflows, but also by tidal forcing, with net circulation being a
65 combined balance from all these variables (Monbet, 1992; Niedda & Greppi, 2007). Turbidity
66 Maxima Zones (TMZs) are prominent features in many meso- (e.g., Tamar Estuary in UK), macro-
67 (e.g., Gironde Estuary in France) and hyper-tidal range (e.g., Severn Estuary) estuaries. These
68 zones are defined as regions with considerable higher suspended solid concentrations above typical
69 background levels (Uncles et al., 1985; Dyer et al., 2002; Manning et al., 2010), primary due to
70 enhanced sediment re-suspension related to shear along the estuarine bed (and, to a lesser extent,
71 salinity induced flocculation) near the landward limits of salt intrusion or within the freshwater
72 zone (Schubel 1968; Uncles & Stephens 1998; Burchard et al., 2018). TMZ formation (including
73 extent and location) is commonly attributed to mechanisms such as tidal asymmetry, and
74 turbulence damping effects (Lin & Kuo, 2001) which all contribute to net estuarine circulation.
75 Net estuarine circulation is the residual circulation at specific estuarine location. Prediction of net
76 estuarine circulation has been an important challenge since the 1950's (Stommel & Farmer, 1953;
77 Hansen & Rattray, 1965; Nunes-Vaz et al., 1990; Li & O'Donnell, 2005). Long-term mean residual
78 circulation is a complex interplay of freshwater inputs, prevailing wind conditions, oceanic tides,
79 local topography bathymetry, and geomorphology, and (in larger areas) Coriolis forcing related to
80 Earth's rotation (Wijeratne & Rydberg, 2007). Sub-tidal barotropic and baroclinic motions play

81 an important role in net estuarine circulation in deeper estuaries with moderate to high tidal ranges
82 (Liungman et al., 2001; Souto et al., 2003).

83 The formation of a TMZ in estuaries with energetic tidal flows (Dyer 1986) is governed,
84 to a large degree, by tidal conditions and tidal asymmetry (Allen et al., 1980; Postma, 1980;
85 Burchard et al., 2018). Tidal asymmetry is mainly related to the bathymetry and topography of an
86 estuary, which can distort the tidal curve and lead to net transport of sediments towards the head
87 of the estuary. This residual transport, known as tidal pumping, is more significant than residual
88 estuarine circulation in estuaries of high tidal range, and its interaction with both sediment settling
89 and resuspension and re-entrainment during the tidal cycle produces and maintains the TMZ.
90 While the TMZ in macrotidal estuaries has often been attributed primarily to tidal asymmetry, with
91 the TMZ location controlled by the tidal-pumping magnitude, some studies have emphasized the
92 importance of both tidal asymmetry and residual circulation in controlling TMZ formation,
93 location, intensity and extent (Allen et al. 1980; Kirby & Parker 1982; Uncles et al., 2002).

94 A close-up view into a typical estuarine TMZ reveals sedimentary mixtures affected by
95 flocculation, a process whereby cohesive and fine-grained mixed sediment particles have the
96 potential to aggregate into flocs (Winterwerp & van Kesteren, 2004; Mehta, 2013). Flocculated
97 muddy sediments often significantly contribute to both the formation of concentrated near-bed
98 suspension layers and TMZs within tidal estuarial waters (Horemans et al., 2020), thus altering
99 turbulent mixing in the water column. Cohesive sediments that are mixed into a predominately
100 cohesionless sandy region can create a “cage-like” structure, thereby trapping the sand within a
101 clay-floc envelope (Whitehouse et al., 2000). The size of flocs ranges from microns to centimeters,
102 and their settling velocity is significantly greater than the constituent particles, while their effective
103 density generally decreases with size (Tambo & Watanabe, 1979; Spencer et al., 2010; Zhang et
104 al., 2018). Macroflocs (diameter (D) > 160 μm) are the most important sub-group of flocs, as their
105 fast-settling velocities, typically of the order of (5-10) mm s^{-1} (Manning & Dyer, 2007; Soulsby et
106 al., 2013), tend to have the most influence on the mass settling flux (Mehta & Lott, 1987). Further,
107 the TMZ encompasses a zone where the physio-chemical and compositional properties of the water
108 changes rapidly from those of fresh water to those of sea water, thus underlining the important role
109 of the floc dynamics in the estuarine region (Dyer, 1989).

110 Although TMZs are typically associated with tidal forcing in meso-, macro- and hyper-
111 tidal range (e.g., Severn Estuary) estuaries, less prominent and ephemeral, storm-induced TMZs
112 also occur and have been documented in microtidal systems (Chen et al., 2018). These less
113 prominent and ephemeral TMZs play an important role in determining net sediment accumulation
114 and transport in estuarine characterized by lower tidal energy. As an example, Geyer et al. (2001)
115 showed that net sediment transport in the micro-tidal lower Hudson River estuary is landward,
116 from the sea into the estuary, with sediment trapping and accumulation patterns mainly controlled
117 by the magnitude of freshwater flow in relation to the modulation effect of the tides. When the
118 spring tide coincides with episodic high-river discharge, net sediment export from the estuary to
119 the sea occurs (Geyer et al., 2001).

120 In contrast to TMZs in highly dynamic estuarine regimes with moderate to high tidal
121 ranges, ephemeral TMZs in microtidal estuaries are less studied, especially in case of microtidal
122 environments (MTEs) with little water exchanges between river and sea (i.e. little tidal prism) with
123 a lower frequency of conditions that are conducive to TMZ development. The investigation on
124 TMZ-related processes and net landward vs. sediment transport in the lower Hudson River estuary

125 conducted by Geyer et al. (2001) was in an MTE characterized by a tide range slightly larger than
126 1 m, but with a quite important tidal prism.

127 This work presents observational data collected from the Misa River (MR hereafter)
128 estuary, a MTE located on the northeast coast of Italy bordering the western Adriatic Sea that is
129 characterized by little river-sea water exchange and a tidal prism of order $\sim(10-100) \text{ m}^3$ during
130 wintertime quiescent periods, stormy, and transitional periods between storms. The data collected
131 are used to describe the hydrodynamics, morphological bed evolution, and water physio-chemistry
132 of the MR under these different conditions along with results of simulations of flocculation
133 dynamics using an existing model suite. In terms of novelties and main goals, the present work
134 aims to: 1) investigate ephemeral TMZ formation and identify conditions under which a TMZ
135 generates in a MTE, here represented by the MR estuary; 2) identify the main contributing factors
136 that lead to TMZ formation and influence ephemeral TMZ localization, intensity, and extent;
137 3) characterize ephemeral TMZ generation under different forcing conditions in terms of physio-
138 chemical parameters and flocculation, and understand how these factors influence TMZ location,
139 intensity, and extent and net sediment transport through the MTE.

140

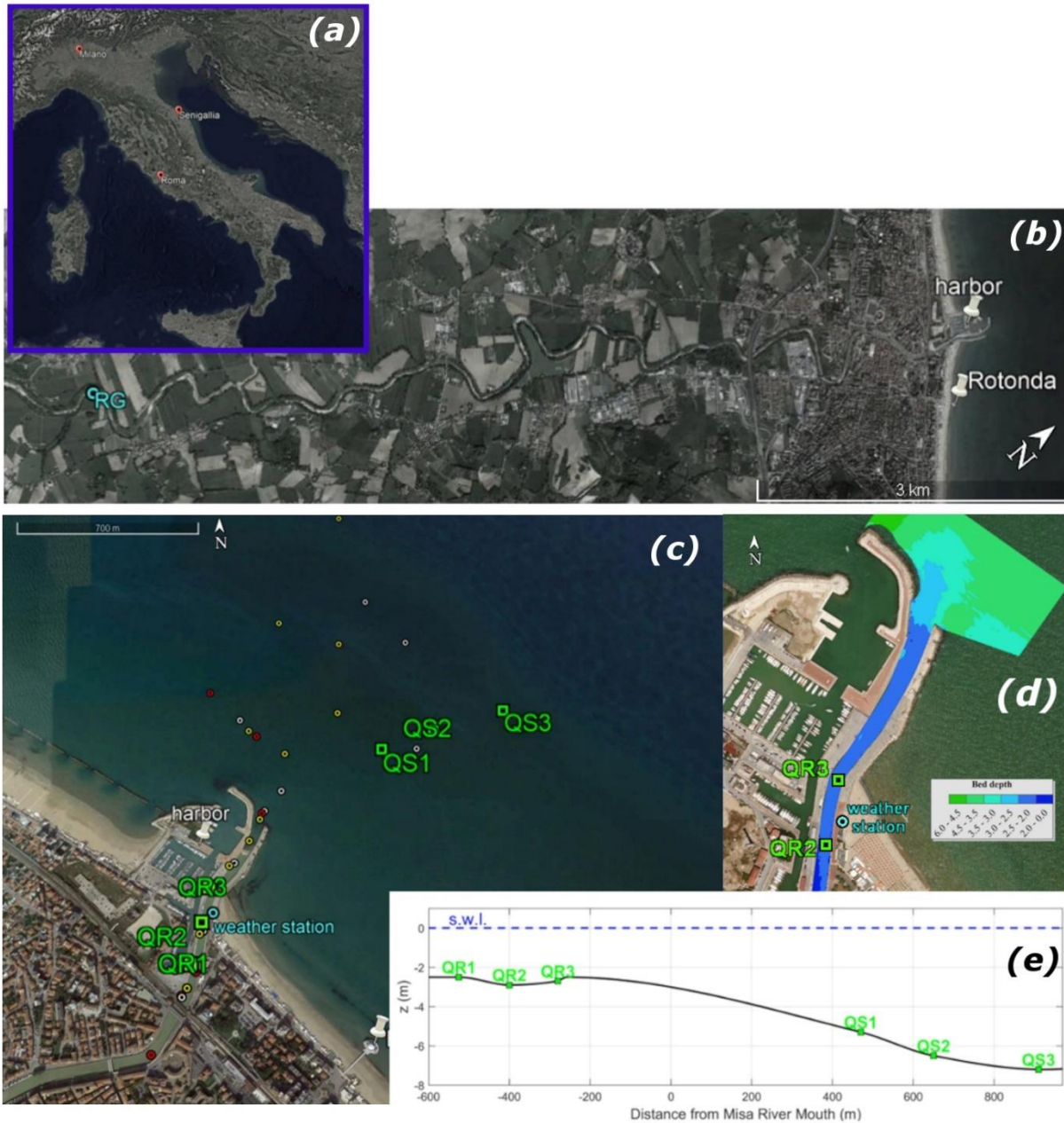
141 **2 Materials and Methods**

142 *2.1 Field Site*

143 The MR originates in the Apennine Mountains (“Appennino umbro-marchigiano”), runs
144 over a watershed area of $\sim 383\text{km}^2$ for ~ 48 km, and flows into the northeastern Adriatic coast of
145 Italy. The final reach passes through the municipality of Senigallia (Marche Region) and is heavily
146 engineered, being comparable to a field-scale laboratory. The beach to the north of the estuary is
147 protected by breakwaters, while the southern part is a natural open coast (Figure 1).

148 Falling into the MTE category, the MR is such that the tidal currents are small (Melito et
149 al., 2020), with the tide range rarely exceeding 0.6 m. Tidal amplitudes observed in January 2014
150 in the port of Ancona (~ 25 km South of Senigallia) were ~ 0.25 m during neap tides and ~ 0.45 m
151 during spring tides¹. During such periods, the diurnal K1 constituent was larger than the semi-
152 diurnal M2, with amplitudes of ~ 0.15 m and 0.07 m, respectively (Pawlowicz et al., 2002). The
153 tidal excursion can reach more than 2 km inland (Brocchini et al., 2015; Postacchini et al., 2020,
154 2022). Similar to many Mediterranean estuaries, that of the MR is a salt-wedge estuary (Kennish,
155 2019) during periods of high river discharge, when the freshwater input prevails over the lower
156 tidal forcing. During these episodic periods, a stratified gradually thinning freshwater layer flows
157 gravitationally downriver over a seawater tongue that extends landward up the estuary. A statistical
158 analysis of available hydrodynamic data allowed for a discharge estimate of ~ 400 and $\sim 600 \text{ m}^3\text{s}^{-1}$
159 for return periods of 100 and 500 years, respectively (Brocchini et al., 2017). A reduction of
160 freshwater flow is expected for the MR in the future, due to climatic variability and human
161 activities in Central Italy (Darvini & Memmola, 2020).

¹ Data available at <https://www.mareografico.it/>



162

163 *Figure 1 – (a) Italy map. (b) Location of the river gauge (RG). (c) Study area of winter experiments (Senigallia, Italy), with*
 164 *location of quadpods in the river (QR) and sea (QS), and sampled stations referring to 26 (white circles), 27 (yellow circles) and*
 165 *29 (red circles) January 2014. (d) Bathymetric survey of the estuarine area before the experiment. (e) Bed elevation within river*
 166 *(negative x values) to sea (positive x values).*

167 The MR contains and distributes large quantities of sediment, with the grain size at the
 168 estuary ranging from clay sizes to cobble and the fine sediments being characterized by strongly
 169 cohesive montmorillonite clay minerals (2-5 μm in size). Episodic sediment and enhanced
 170 suspended load transport from the Apennine Mountains towards the MR mouth and into the coastal
 171 western Adriatic Sea is forced by heavy rains leading to higher river discharge that typically occur
 172 as the frequency and intensity of Bora winds increase and as the temperature difference between

173 Sirocco winds and air masses in the northern Adriatic Sea increases (Milliman & Syvitski, 1992).
174 The total sediment discharge from the mouth of the MR estuary is estimated to be $8.4 \cdot 10^8 \text{ kg yr}^{-1}$
175 (Frignani et al., 2005) and $4.7 \cdot 10^8 \text{ kg yr}^{-1}$ for the suspended load (Milliman & Syvitski, 1992).
176 Once the Apennine river-sourced sediments discharge into the nearshore zone of the Western
177 Adriatic, alongshore sediment transport is dominant over cross shore. Apennine river sediments
178 are primarily transported southward by the Western Adriatic Coastal Current (WACC), enhanced
179 by the winter Bora and during the relaxation of Sirocco winds (Fain et al., 2007, Orlic et al., 1992),
180 while the Deep-Water Outflow Current (DWOC) transports sediments discharged by Alpine rivers
181 through the central portion of the Adriatic Sea (Tomadin, 2000; Colantoni & Mencucci, 2010).

182 **2.2 2014 Field Experiment**

183 A field experiment was executed in the MR estuary in January 2014 (Figure 1). The
184 experiment was aimed at understanding the main estuarine processes occurring during the winter
185 in this representative MTE by collecting hydrodynamic, morphological and physio-chemical data
186 (for details, see Brocchini et al., 2015; 2017). To monitor the range of suspended sediment
187 concentrations, morphodynamic and hydrodynamic, and physicochemical conditions during
188 quiescent periods, stormy and transitional period between storms, a wide range of *in-situ*
189 instrumentation was deployed for varying durations from the lower reach of the MR to
190 approximately 1 km offshore of the mouth.

191 Due to the combined factors of deployment duration, ambient conditions expected during
192 winter measurements, remote instrumentation recording, and minimizing the disturbance of the
193 water column (in particular any developing interfacial gradients), the majority of the sensors were
194 acoustic based. The hydrodynamics of the system was observed using five bottom moorings called
195 quadpods (Figure 2), with each of them having a dedicated instrumentation suite. Similar to recent
196 field campaigns (e.g., Klammer et al., 2021), four large square plates of $(49 \times 49) \text{ cm}^2$ were placed
197 at the four corners of the base to prevent the quadpods from sinking in soft sediments (mainly silt
198 and some gravel in the final reach of the MR, fine sand in the nearshore area) and to provide a
199 location for weights to prevent the quadpods from being disturbed or mobilized by large waves or
200 currents. The onboard compass and constant recording of pitch and roll were also used to check
201 eventual mobilization of the quadpods. Each quadpod covered 1 m^2 at the base and was 1 m in
202 height.

203 The five quadpods were deployed at six different locations within the river, approximately
204 in the middle of the cross-section (i.e., QR1, QR2, QR3), and in the sea (i.e., QS1, QS2, QS3), as
205 illustrated in Figure 1c. The use of a crane and divers allowed the quadpods to be readily moved
206 and redeployed along the river. Specifically, two quadpods were initially deployed at QR1 (~530 m
207 upriver of the mouth) between 22 and 24 January, and then moved to QR2 (~400 m upriver of the
208 mouth) between 24 and 29 January. A third quadpod was deployed at QS1 (~460 m offshore, at
209 ~5-m depth) between 23 and 27 January. The fourth quadpod was first deployed at QS2 (~640 m
210 offshore, at ~6-m depth) between 23 and 27 January, and then moved to QR3 (~290 m upriver of
211 the mouth) between 27 and 29 January. The fifth quadpod was constantly measuring at QS3
212 (~900 m offshore, at ~7-m depth) between 23 and 29 January (Figure 1c).



Figure 2 – One of the quadpods deployed in the MR.

213
214

215 A bathymetric survey carried out few days before the experiment (Figure 1d) and a long-
216 river/cross-shore profile extracted from the instrument recordings (Figure 1e) better show the pod
217 locations and the bed elevation in the study area. Since the final reach of the MR is highly
218 engineered, the cross-sections are almost rectangular and fairly uniform between QR1 and QR3
219 locations, their widths being ~20m. Moving downriver, the width increases, reaching almost 40m
220 at the mouth. In terms of bed elevation, although this globally tends to decrease between QR1 and
221 the mouth, a small bed perturbation is visible just downriver of QR3 (Figure 1e), which gave rise
222 to a river mouth bar in the years following the experimental campaign (Baldoni et al., 2021).

223 Observations made at QR2 and QS2 were used for the analysis of a big Bora storm (BS
224 hereafter) occurring during 24-25 January 2014, while those located at QR2 and QR3 were used
225 for the analysis of a smaller storm (SS hereafter) occurring during 28-29 January 2014. Table 1
226 summarizes the instruments used for the analysis of the observed ephemeral TMZ, with related
227 locations and operation times. The flow velocity across the lower portion of the water column (a
228 bit more than 1 m from the bed) was collected at both river quadpods and QS2, which were
229 equipped with two velocity profilers (Nortek HR Aquadopp, 2 MHz, sampling at 2 Hz for 45
230 min/h), the seabed location was recorded by a pencil-beam sonar (Imagenex 881A, sampling at 1
231 MHz and scanning 10 lines per hour, orientation fixed with the pod, straight line profiling and
232 sonar working as an altimeter) and the surface level was detected by a pressure sensor (sampling
233 at 2 Hz for 45 min/h). The velocity profilers were programmed with a 10-cm blanking distance,
234 with an uplooking profiler with bin size of 5 cm and a down-looking profiler with bin size of 2 cm
235 (40 total bins in the combine profile), while the overlap region between the velocity profilers
236 occurs near 0.4 m above the bed. QS3 was only equipped with an ADCP which enabled the
237 recording of the wave characteristics every hour (see also Brocchini et al., 2017).

238 Additional observations of environmental conditions during the field experiment were used
239 in the analysis that follows. First, data collected by a weather station located on top of the harbor
240 lighthouse (Figure 1c) was used to quantify wind speed and direction and precipitation. To better
241 quantify the river forcing and estimate the timing of peak discharge, the river stage was measured
242 every half an hour by the river gauge (RG hereafter) located at the Bettolle station (Figure 1b).
243 The RG is located about 10 km upriver of the MR mouth and was the closest to the mouth among
244 all hydrometers existing along the MR during the experiment (see also Melito et al., 2020).

245 Water and sediment samples were collected from the MR estuary from a small boat during
246 quiescent periods between or immediately following storm events when safe weather conditions
247 were ensured. Water column observations were carried out once per day at several stations (see

248 Figure 1c) during the period between the two storms on the morning of 26 January 2014,
 249 approximately between 11.00 and 14.30 (white circles) and 27 January 2014, approximately
 250 between 10.00 and 13.00 (yellow circles). Similar sampling was conducted immediately after the
 251 SS on the morning of 29 January 2014, approximately between 10.00 and 13.30 (red circles).
 252 Observations spanned more than 1 km along the final 700 m of the MR out to about 500 m offshore
 253 of the MR mouth. Vertical profiles of temperature, pH, salinity, and turbidity were logged at select
 254 locations at 0.5 m depth intervals using a pre-calibrated Hach Quanta Hydrolab® water quality
 255 sonde. Details on sediment type and median grain size are presented in Brocchini et al. (2017).

256

257 *Table 1. Instrumentation deployed during January 2014 experiment and used for the present work (see also Brocchini et al.,*
 258 *2017).*

| <i>Operation Time</i> | <i>Location</i> | | <i>Instrument</i> | <i>#</i> |
|---|---|------------------------|--|-------------|
| 24-25 January (BS) | -400m | QR2 | Velocity profilers Pencil-beam sonar Pressure sensor | 2 1 1 |
| | +640m | QS2 | Velocity profilers Pencil-beam sonar Pressure sensor | 2 1 1 |
| 28-29 January (SS) | -400m | QR2 | Velocity profilers Pencil-beam sonar Pressure sensor | 2 1 1 |
| | -290m | QR3 | Velocity profilers Pencil-beam sonar Pressure sensor | 2 1 1 |
| 24-25 January & 28-29 January (BS, transition, SS) | +900m | QS3 | ADCP | 1 |
| | -10km | RG | hydrometer | 1 |
| | lighthouse near MR mouth | weather station | - | 1 |
| | Ancona harbor, 25 km South of Senigallia | tide station | - | 1 |

259

260 Water sampling and relevant measurements were used to estimate additional terms useful
 261 for a spatio-temporal description of the estuarine stratification during the field experiment.
 262 Specifically, water density in the MR estuary was reconstructed on the basis of pressure,
 263 temperature and salinity² (Gill, 1982), which were obtained from the water samples and cast data.
 264 Based on these data and results, a stratification parameter was estimated as:

$$265 \quad \eta_S = \frac{\Delta S}{S_m} \quad (1)$$

266 where ΔS is the difference between bottom and surface salinity values, and S_m is the average
 267 between bottom and surface salinity. The water column is well-mixed when $\eta_S < 0.1$, partially
 268 mixed if $\eta_S = (0.1 - 1)$ and stratified for $\eta_S > 1$ (Prandle, 2009; Restrepo et al., 2018).

² Gabriel Ruiz-Martinez (2022). Seawater density from salinity, temperature and pressure
<https://www.mathworks.com/matlabcentral/fileexchange/85900-seawater-density-from-salinity-temperature-and-pressure>, MATLAB Central File Exchange. Retrieved January 31, 2022.

269 **2.3 Flocculation model**

270 Since the flocculation is one of the main mechanisms controlling the fate of fine sediments
271 and contaminants in estuaries (Manning et al., 2010), its understanding is strongly related to the
272 TMZ formation. To investigate the potential relative depositional effects leading to the TMZ
273 formation within the MR and due to the lack of floc settling measurements during the field
274 campaign, an existing flocculation model (FM) suite was used (Manning & Dyer, 2007; Spearman
275 & Manning, 2008; Manning et al., 2011). The FM is based on actual floc settling velocity and floc
276 mass distributions (approximately 200 floc populations) from a wide range of turbulence and SSC
277 conditions, and flocs are composed from different sand-mud mixtures. The approach follows the
278 concept of macroflocs (size>160 μm) and microflocs (size<160 μm)(Krone, 1963; Eisma, 1986),
279 whereby the former floc type is constructed from the latter. The input parameters include SSC,
280 sediment type/mixture, and turbulent shear stress, while the outputs include macrofloc settling
281 velocity (W_{SMACRO}), microfloc settling velocity (W_{SMICRO}), ratio of floc mass between the two size
282 fractions ($\text{SPM}_{\text{ratio}}$), and the total mass settling flux (MSF), as outlined in Appendix B.1.

283 The FM was applied to the MR estuary through assessment of three scenarios, i.e. SS, BS
284 and transition between the storm events. Spatially, three points along the MR transect were
285 considered: i) inland (~500m upriver of the mouth); ii) mid-zone (approximately at the mouth);
286 iii) seaward region (~500m offshore of the mouth). Depth-wise focused on two profile points were
287 chosen at each location, 0.25 m above the bed, where flocculation tends to be highly significant
288 (Mehta & Lott, 1987), and a local mid-depth position. To run the FM, suitable input values are
289 needed. To this aim, the SSC range was obtained from a relative comparison from the turbidity
290 measured during the water and sediment samples. High SSC values are in the region of 2,500 mg/L
291 and for this scenario comparison assessment, this was deemed equivalent to the peak measured
292 250 NTUs. Hence, the NTUs at each scenario assessment point were nominally converted to SSC
293 equivalent values using 1 NTU = 10mg/L (see also the experimental findings at Section 3.3).

294 The suspended sediment composition at each location was based on both previous MR
295 studies and samples taken during January 2014 (Brocchini et al., 2015, 2017). For the FM, the
296 following nominally representative mud:sand (M:S) compositions were considered: both 100M:0S
297 and 75M:25S at the inland (TMZ) site, 50M:50M equal mud/sand mixture at the mid-zone, and it
298 was assumed to be pure sand (0M:100S) in the seaward region. The level of flocculation primarily
299 depends upon the combined effects of SSC and turbulent mixing. To provide a comprehensive
300 assessment of flocculation, the turbulent shear stresses at each location used by the FM were based
301 on a range typically experienced in many tidal estuarial locations: 0.06, 0.35, 0.6, and 0.9 Pa.
302

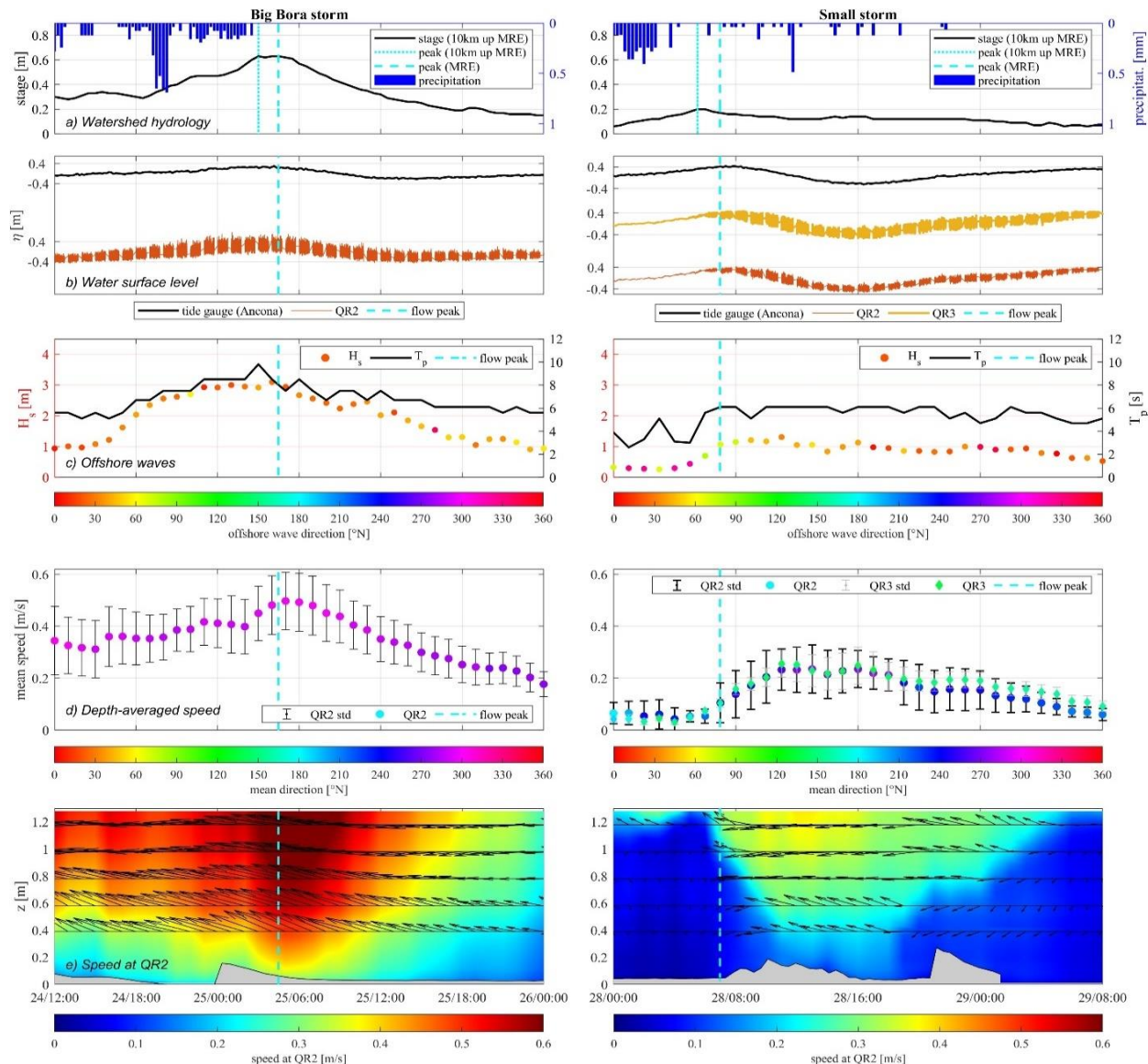
303 **3 Results**

304 During the observational period of the field experiment, two winter storms occurred from
305 24-25 January 2014 and 28-29 January 2014, respectively. The former storm (BS) was
306 characterized by high energy waves and was mainly driven by NNE winds (Bora), while the latter
307 storm (SS) was driven by less intense winds coming from NNW. River discharge was significantly
308 different during the two events.

309 **3.1 Big (Bora) storm versus small storm**

310 Figure 3 summarizes observations made during the storms that occurred on 24-25 January
311 2014 (BS) and 28-29 January 2014 (SS) at QR2. Figure 3a shows mean precipitation in the

312 watershed and the river stage observed at the Bettollelle station, ~10 km upriver of the mouth. The
 313 timing of the peak stage at the Bettollelle station and at the mouth is indicated (vertical light blue
 314 lines). The time for the peak stage to travel from Bettollelle station to the station of Ponte Garibaldi
 315 (~1.5 km upriver of the mouth and operating since 2016) was ~1.25 hr during flood events
 316 recorded in 2018 (Melito et al., 2020). Consequently, for this work, the time for the peak stage to
 317 travel from Bettollelle station to the mouth was estimated ~1.5 hr as well.



318

319

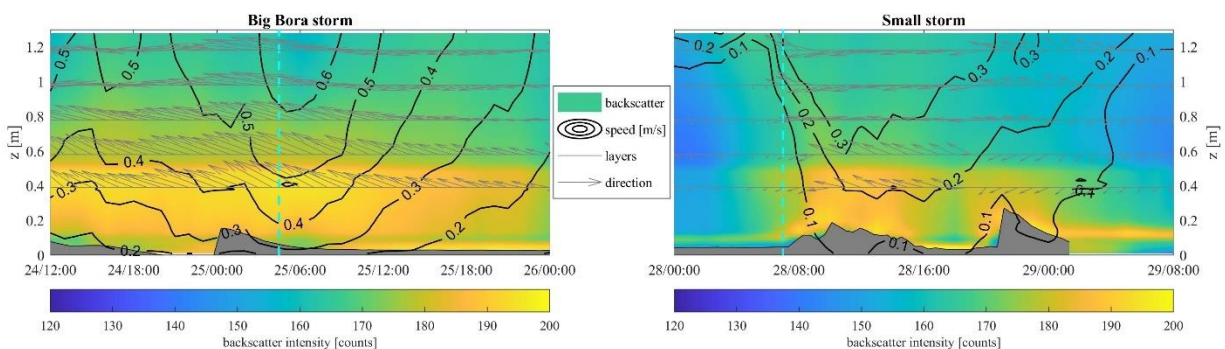
320 *Figure 3 – Observed environmental conditions for BS (left panels) and SS (right panels). a) Mean precipitation in the watershed*
 321 *(blue bars) and stage at Bettollelle (~10km from the MR mouth, black line). b) Water surface level recorded by tide gauge*
 322 *(Ancona, black line) and sensors at estuary (QR2, orange line; QR3, yellow line). c) Significant wave height and incoming*
 323 *direction (colored dots), and peak period (black line) at QS3. d) depth-averaged speed with mean direction (colored symbols)*
 324 *and standard deviation (error bars) at QR2 and QR3. f) Vertical distribution of speed, with direction shown by arrows at QR2*
 325 *(upward indicates north), and bed estimates (w.r.t. quadpod deployment) from pencil beam sonar (grey areas). In each panel,*
 326 *light blue vertical lines indicate the timing of the flow peak at Bettollelle (solid) and MR mouth (dashed).*

327 Figure 3b shows the water surface levels observed at the nearby Ancona harbor (black
 328 lines), which provides surge and tidal data applicable to the Senigallia area with negligible delay

329 (Brocchini et al., 2017). The instantaneous water levels observed at QR2 (red lines) and QR3
 330 (yellow line) are also shown. The wave conditions are illustrated in Figure 3c showing significant
 331 height H_s (circles), peak period T_p (black lines) and peak direction (colors of circles, see color bar).
 332 Figure 3d illustrates both mean speed (refer to vertical axes) and direction (refer to color bars)
 333 observed by the Aquadopps at QR2 (circles) and QR3 (diamonds). The values are depth-averaged
 334 along the considered depth and are represented together with their standard deviation (black error
 335 bars for QR2, gray for QR3), which describes the (more or less pronounced) vertical variation of
 336 the horizontal speed.

337 Figure 3e illustrates the hourly-averaged speed along the water column observed at QR2.
 338 The speed directions (upward indicates north, i.e. 0°) at four horizontal layers are also shown using
 339 black arrows. However, such speeds are not perfectly downriver (the river orientation at QR2
 340 suggests a direction slightly larger than 0° N, as shown in Figure 1d), because the collected data
 341 only refer to the lower water column (the total water depth being ~ 2.5 m at QR2, see Figure 1e)
 342 and because of the generation of secondary/cross-river flows, consequence of the nearby bend
 343 (~ 100 m downriver of QR2). In addition, the momentum induced by the incoming sea waves
 344 contributes differently to the flow directionality during the recorded time, as it can be observed
 345 during the BS or at the SS wave-height peak (high- or moderate-flow conditions) and before or
 346 after the SS wave-height peak (low-flow conditions). Although measurements in the upper water
 347 column were not collected during the whole experiment, a clear upriver flow (direction in the range
 348 180 - 240° N) was recorded in the lower water column at QR2 during the tail of the SS (latest stages
 349 plotted in Figure 3d) and quiescent conditions (see section 3.4), this suggesting a region with large
 350 shear in the mid water column, which connects an upriver flow (lower column) with a downriver
 351 flow (upper column).

352 To better quantify the turbidity during the two events, the backscatter amplitude is
 353 illustrated in Figure 4. While it is possible to estimate the magnitude of suspended particulate using
 354 the backscatter amplitude, a separate, direct measure of sediment concentration is needed to
 355 calibrate the backscatter across the profile. Lacking the additional measurements needed to
 356 perform a calibration, we have applied a de-meaning approach to each bin of each beam separately,
 357 to remove beam pattern and environmental biases, as successfully applied to multibeam
 358 echosounder data (de Moustier & Kraft, 2013). Such result more accurately represents the relative
 359 magnitudes (i.e., gradients) of SSC across the profile, which are more consistent with the sonar
 360 saturation observed at QR3 (see section 3.2).



361
 362 *Figure 4 – Observations during BS (left panels) and SS (right panels) were made at QR2 for the acoustic backscatter intensity*
 363 *along the water column (color maps), speed (contour lines) and velocity directions (arrows). The location of the riverbed*
 364 *estimated from hourly averages of the pencil beam sonar line scans is overlaid in grey.*

365 Observations at QR2 during BS show that high seaward river discharge through the estuary
 366 (stage ~0.6 m at Bettollelle) competed with significant landward forcing from the sea (wave height
 367 >3 m at QS3 and >0.5 m at QR2 recorded during high tide) at the estuary (Figure 3a-c, and Melito
 368 et al., 2020). As a result, the longitudinal flow direction along the water column was downriver
 369 but there was also some secondary circulation, with a depth-averaged speed ~0.5 m/s during the
 370 peak (Figure 3d-e). The high backscatter observed during the whole BS event suggests large
 371 sediment re-suspension, especially in the lower water column (Figure 4, left panel).

372 The SS resulted in different hydrodynamic conditions in the MR estuary, with moderate
 373 river discharge (stage ~0.2 m at Bettollelle) and milder wave action (wave height ~1 m at QS3 and
 374 <0.1 m at QR2) during the peak (Figure 3a-c), with the wave forcing increasing at the MR mouth
 375 after the peak (~0.3 m at QR2). Hence, depth-averaged speeds were relatively low and the
 376 maximum value (~0.25 m/s) occurred four hours after the peak, suggesting that: 1) river flow was
 377 mostly localized within the upper water column ($z > 1.3$ m, not captured by the observations);
 378 2) an important river-sea interaction occurred (Figure 3e), as also testified both by the modification
 379 of the flow directionality (black arrows) and by the ratio between standard deviation and depth-
 380 averaged speed (~0.45, Figure 3d). Varying directions characterize the water column and strongly
 381 change with time, with inflowing at lower layers and outflowing at the upper layers during the
 382 flow peak/high tide and during the following flood tide (around 20:00 of 28 January), vice versa
 383 during the low tide (around 16:00). Further, a persistent salt wedge intruded onto the river in the
 384 lower water column with a buoyant river plume in the upper water column at QR3, where the
 385 vertical shear was less evident than upriver (Figure 3d). The high backscatter at QR2 (Figure 4,
 386 right panel) testifies that a high turbidity remains within the lower water column ($z < 0.7$ m) for
 387 about 16 hours (from 28/01 at 8:00 to 29/01 at 00:00), i.e. the time during which the offshore wave
 388 height oscillates around 1 m.

389 The comparison between BS and SS in terms of energy and energy flux in the offshore
 390 region (i.e., at QS3) is illustrated by the following equations:

$$391 \left(\frac{H_{s,BS}}{H_{s,SS}} \right)^2 \sim \left(\frac{3}{1} \right)^2 = 9 \quad (2)$$

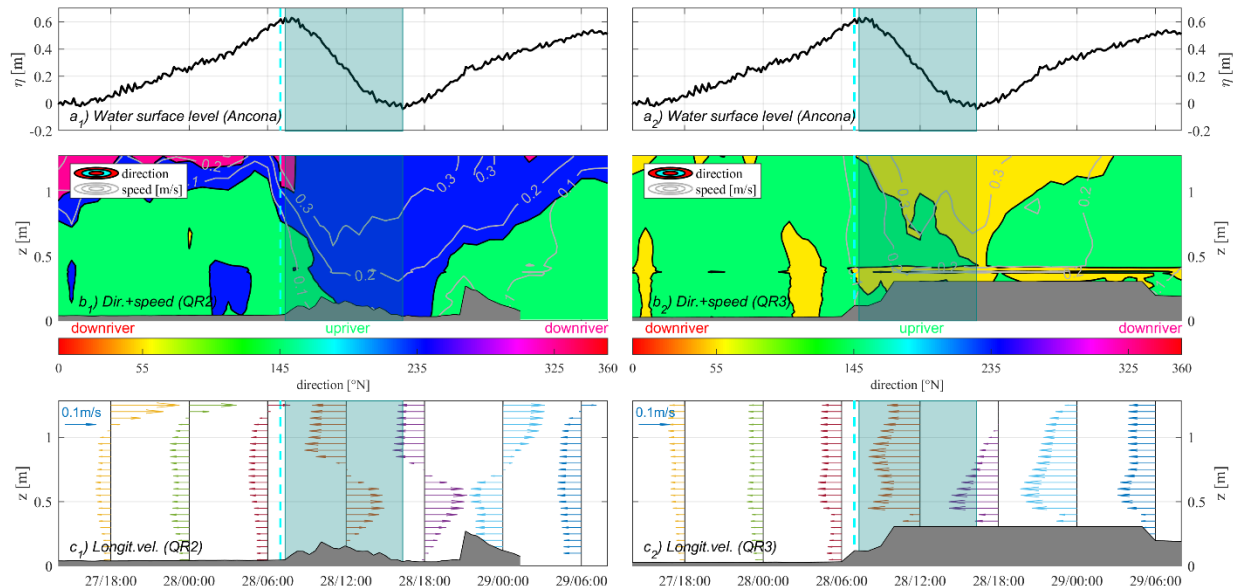
$$392 \left[\left(\frac{H_{s,BS}}{H_{s,SS}} \right)^2 \frac{c_{g,BS}}{c_{g,SS}} \right] \sim \left[\left(\frac{3}{1} \right)^2 \left(\frac{6.8}{3.9} \right) \right] = 16 \quad (3)$$

393 where H_s and c_g represent, respectively, the significant wave height and group speed estimated
 394 offshore during BS and SS. Eq.2 is the ratio between the wave energy estimated during BS and
 395 the wave energy during SS, showing that the offshore energy is 9 times larger during the BS than
 396 during the SS. Similarly, eq.3 gives the ratio in terms of energy flux, revealing that such quantity
 397 is 16 times larger during BS. Moreover, a strong energy decay occurred at the estuary during the
 398 BS peak, although only a slight dissipation characterized the wave propagation from QS3 to QS2.
 399 Specifically, the total significant height drops to $H_{s,BS} \sim 0.5m$ at QR2 (about 17% of that recorded
 400 at QS3), mainly due to the strong breaking close to the mouth that provided a large drop of the
 401 sea-swell component, while the lower-frequency/infragravity waves were almost unaffected and
 402 propagated upriver almost unaltered (Melito et al., 2020). Much smaller is the dissipation during
 403 the SS, when the total significant height drops to $H_{s,SS} \sim 0.3m$ at QR2 (about 30% of that recorded
 404 at QS3). Hence, although the reduced wave energy coming from the offshore during the SS, a
 405 smaller breaking at the mouth promoted the wave penetration within the MR, which is also
 406 facilitated by the less intense river flow. Such occurrences contributed to: i) a pronounced

407 interaction between river and sea, ii) a high turbidity and stratification within the final reach of the
 408 MR (see also implications in terms of flocc dynamics at Section 3.4), iii) the generation of a
 409 convergence zone between QR2 and QR3.

410 3.2 Characterization of the small storm

411 During the SS, observations in the lower reach of the MR suggest the persistence of a
 412 density gradient that was modulated in space (between QR2 and QR3) and time by the local surge,
 413 as testified by the signature of a buoyant river plume, evident in the uppermost recorded region.
 414 Specifically, before the flow peak (light blue vertical line), at QR2 there was a stronger, more
 415 coherent downriver current in the upper water column ($z > (1-1.2)$ m, purple region in Figure 5b₁),
 416 a thin layer of cross-river flow, bending leftward, just below ($z > (0.8-1)$ m, blue region) and a
 417 weak upriver (sea intrusion) current (< 0.1 m/s) in the lower water column ($z < (0.8-1)$ m, green
 418 region). Conversely, before the flow peak at QR3, the current was nearly stagnant (< 0.1 m/s) with
 419 mean direction nominally upriver across the vertical (green region in Figure 5b₂), but characterized
 420 by oscillations and larger variance, with occurrence of some cross-river/secondary flows in the
 421 range (55-140)°N (yellow regions). A clearer view of the longitudinal velocity components is
 422 provided in Figure 5c₁, c₂, where rightward/leftward arrows represent the downriver/upriver flows.
 423 At both locations, the backscatter exhibited a vertical gradient with a maximum at the bed (e.g.,
 424 see Figure 4b for what concerns QR2, not shown for QR3). Here, the maximum backscatter value
 425 at QR2 (~170) was a bit smaller than the value at QR3 (~200).



426
 427 *Figure 5 – Data collected during the SS. a) Water surface level measured by the tide gauge (Ancona). b) Speed (contour lines)*
 428 *and velocity directions (color map) at QR2 and QR3. c) Longitudinal velocity component (between 27/01/2014 at 18:00 and*
 429 *29/01/2014 at 06:00, every 6 hr). The location of the bed estimated from hourly averages of the pencil beam sonar line scans is*
 430 *overlaid in grey. Shaded areas highlight the period during which ebb tide occurred.*

431 After the peak stage (shaded area), the horizontal velocity followed the tide evolution, with
 432 the flow direction in the lower part changing from mainly upriver (green) to mainly cross-river
 433 (blue) at QR2, and the cross-river flow extending to the bed during the low tide (Figure 5b₁).
 434 Looking at the longitudinal components, the ebb tide and part of the flood tide are dominated by

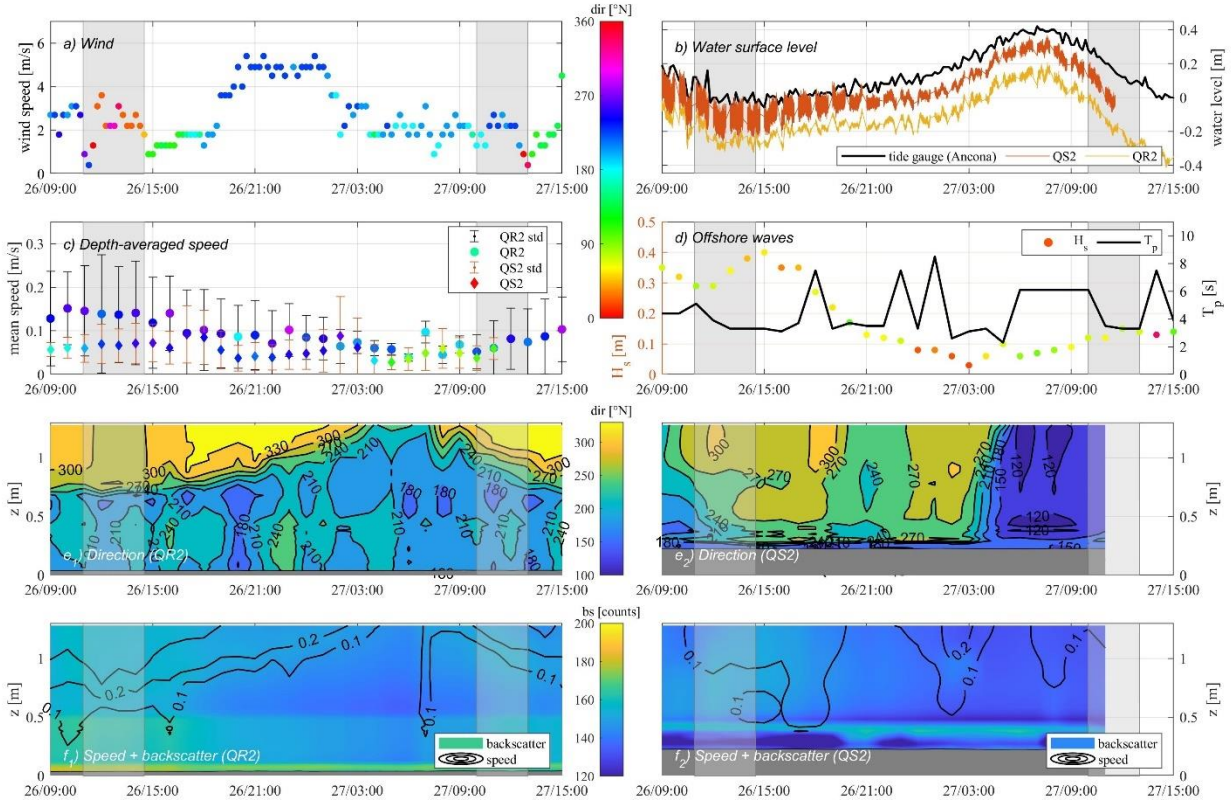
435 an interplay between river forcing and sea waves (orange and purple profiles in Figure 5c₁), which
436 modified the classical seawater-intrusion pattern observed before and after the storm (see also
437 Appendix A.1), and significantly affected the riverbed evolution, as testified by the sonar
438 recordings (gray region). A near-bed stratification is highlighted by the backscatter signal during
439 the ebb and following flood tide (Figure 4b, yellow tones).

440 The sea action was predominant at QR3, with the tide modulating the generation of cross-
441 river/secondary flows (Figure 5b₂), observed all along the lower water column. Further, downriver
442 flows were almost negligible, while the sea waves played a major role and forced the flow to
443 propagate upriver (Figure 5c₂). In agreement with the backscatter increase, the pencil beam sonar
444 detected the onset of sediment deposition at 06:00 on 28 January (just prior to the peak flow), then
445 the bed level kept growing until the blanking distance of the pencil beam was exceeded (around
446 10:00) and started to decrease when the SS began to subside (morning of 29 January). Sediment
447 deposition was evident during the mechanical recovery of QR3 (Brocchini et al., 2017), and is
448 demonstrated by the water elevations observed at QR2 and QR3 (Appendix A.2).

449 **3.3 Water and sediment samples**

450 During the post-storm to quiescent period between the two storms (on 26 and 27 January)
451 and after the SS (on 29 January), *in situ* sampling operations occurred (see Section 2.2). The timing
452 of sampling conducted during the mornings of 26 and 27 January are shown by the shaded areas
453 in Figure 6 to provide context with the overall hydrodynamics. Each sampling period had similar
454 wind speeds (Figure 6a). The first sampling period (26 January) occurred during low tide, with
455 larger wave heights both nearshore (0.3 m to 0.4 m, Figure 6d) and within the estuary (Figure 6b),
456 and larger speeds at QR2 (Figure 6c). The second time period (27 January) occurred during ebb
457 tide, with smaller wave heights (0.1 m to 0.15 m) and smaller mean speeds and standard deviations
458 at QR2. As before (Figure 5b₁), the tide influence was relevant at QR2 (Figure 6e₁, f_1), while the
459 speed close to the bed at QS2 was relatively small during the sampling period (Figure 6f₂), with
460 directions rapidly changing (Figure 6e₂), in agreement with the wave direction (Figure 6d).

461 Riverbed samples were also collected in the final reach of the MR during the quiescent
462 periods prior to the BS, between BS and SS, and after the SS. Large concentrations of gravel were
463 observed in the central portion of the river, which also contained accumulations of terrigenous
464 organic matter (detrital vegetation) during the whole experiment (e.g., before the BS storm at QR1
465 and after the SS at QR3). The fine-grained sediment within the entire final reach was characterized
466 by fine silt, clay and siliceous minerals, with dominance of montmorillonite. Moving downriver,
467 fine sand was observed starting from the mouth up to the offshore quadpods. The fine sand also
468 dominated re-suspended sediments, which were found in water samples collected between the final
469 reach of the MR and ~1.3 km offshore, i.e. at the plume edge. Flocculated particles were also found
470 in the water column, with the sizes of the natant flocs larger on 26 January than on 27 and 29
471 January, suggesting floc aggregation into larger flocs when the BS/SS subsided, followed by
472 subsequent deposition (Brocchini et al., 2017).

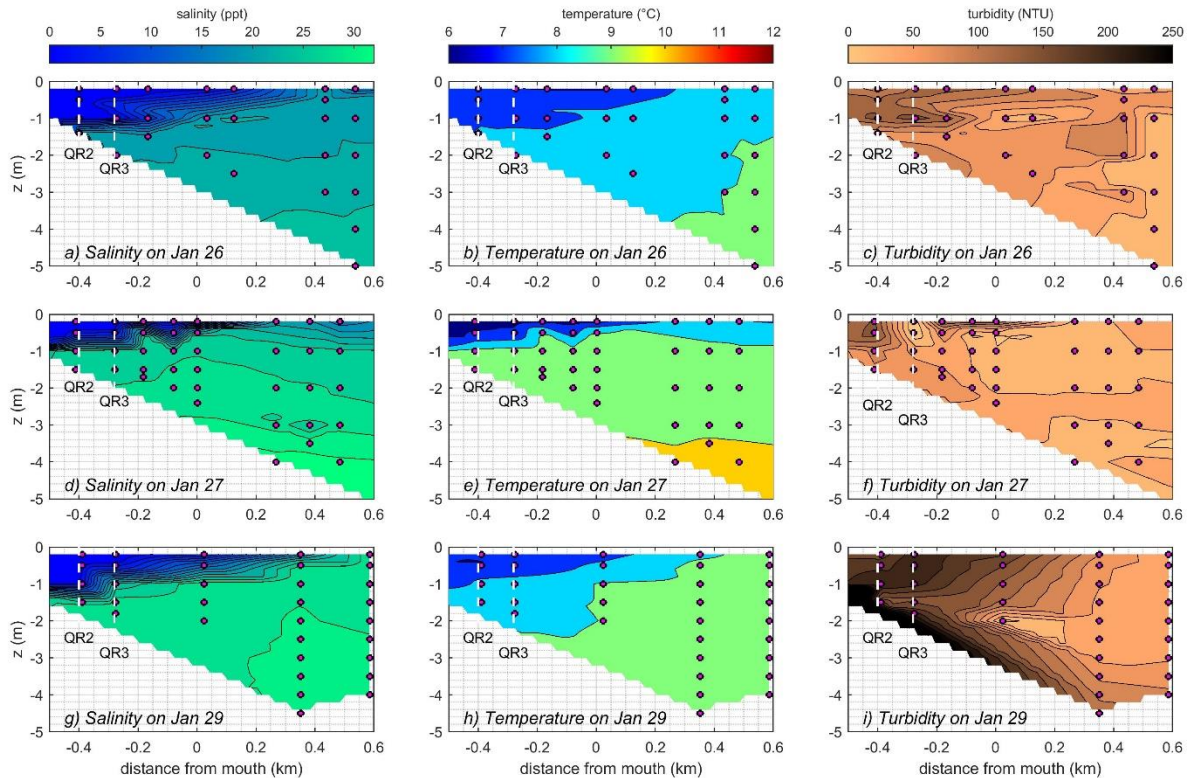


473

474 *Figure 6 – Data collected during the quiescent period. a) Wind at the estuary. b) Water-surface level recorded by tide gauge*
 475 *(Ancona) and sensors at MR estuary (QR2, QS2). c) Depth-averaged speed with mean direction (colored symbols) and standard*
 476 *deviation (error bars) at QR2 and QS2. d) Offshore wave characteristics (QS3). e) Velocity directions at QR2 and QS2. f) Speed*
 477 *(contour lines) and backscatter intensity (color map) at QR2 and QS2. Shaded rectangles give the time during sample collection.*

478 In the beginning of the quiescent period, i.e. during the tail of the BS (26 January), the 3.5–
 479 5 m deep seaward region was generally well-mixed (salinity 22–24 ppt, Figure 7a, temperature 8.5–
 480 9°C, Figure 7b), with just the surface 0.5 m displaying colder, fresher water. Turbidity was less
 481 than 50 NTU, with water sample analysis indicating primarily fine sandy sediments present. About
 482 300 m upriver from the mouth, the depth had shallowed to 2 m, and the likely sediment re-
 483 suspension caused by the higher river flow induced during the BS led to a more than doubling
 484 (~130 NTU) of turbidity (Figure 7c) as compared to observations in the seaward region. The re-
 485 suspended muddier sediments present at -0.3 to -0.6 km zone would exhibit much stronger
 486 flocculation kinetics than the less cohesive (higher sand content) suspension in the MR approaches.
 487 The inland water was cooler (7°C), less brackish (salinity <2 ppt in the surface 1 m), and a sharp
 488 halocline developed within the 1–1.5 m-deep region.

489 The transitional period between the passing of the BS and the run-up to the SS (27 January),
 490 resulted in warmer (~1°C) and more saline (>28 ppt) well-mixed water column conditions within
 491 the MR system (Figure 7d,e). There was some partial stratification with cooler (<8°C), less saline
 492 (<10 ppt) conditions in the (0.5–1) m surface water inland from the mouth of the MR. Turbidity
 493 levels (Figure 7f) were generally halved from those observed during the tail of the BS, ranging
 494 from 25 to 80 NTUs for the seaward and inland regions, respectively. This would equate to a
 495 significant reduction in particle interactions for flocculation, especially in the MR inner region
 496 (between -0.3 and -0.6km), where the higher turbidity levels in the upper water column suggests a
 497 riverine origin for the suspended sediments.



498

499 *Figure 7 – Data from samples (indicated by dots) collected at the estuary on 26 January (top row), 27 January (middle row) and*
 500 *29 January (bottom row): a-d-g) salinity; b-e-h) temperature; c-f-i) turbidity.*

501 The transitional period after the SS during the morning of 29 January promoted partial
 502 mixing in the upper part of the water column through the MR leading to a higher degree of
 503 stratification. This is demonstrated by the steep haloclines formed post SS as indicated salinities
 504 spanning 0-26 ppt in the upper 1 m of the water column (Figure 7g). Warmer (~9°C) (Figure 7h)
 505 seawater encroached 400 m further inland during the SS than during the BS. A notable feature is
 506 the formation of a TMZ (Figure 7i) in the inner MR channel post-SS in a region where the
 507 sediments are seen to be predominantly cohesive (Brocchini et al., 2017). Figure 7i shows a
 508 turbidity gradient progressively building seaward to landward, with maximum turbidity levels
 509 exceeding 180 NTU. Observed turbidity levels approaching 250 NTU (0.3 – 0.5) m above the bed
 510 in the < -0.3 km region suggests the formation of a concentrated benthic suspension (CBS) layer
 511 (Wolanski et al., 1988; Ross & Mehta, 1989); these types of features have been observed in many
 512 traditional estuarine TMZs. CBS layers have the potential to set-up turbulence damping and drag
 513 reduction effects (Best & Leeder, 1993; Li & Gust, 2000; Dyer et al., 2004; Manning et al., 2006),
 514 and importantly, this environment would be highly conducive for stimulating flocculation
 515 (Manning & Bass, 2006; Gratiot & Manning, 2008).

516 **3.4 Indicative flocc dynamics**

517 As described in Section 2.3, a FM was initialized using the turbidity measurements
 518 illustrated in Figure 7, as well as on the analysis described in previous studies (Brocchini et al.,
 519 2015, 2017). To examine the resultant formation of the TMZ and flocculation at each location for
 520 a nominal period of time (as opposed to a continual timeline of stratification generation), the FM

521 output computed at moderate shear stress level of 0.35 Pa was used as a benchmark turbulence
 522 level, in order to facilitate the various scenario intercomparisons and in agreement both with
 523 previous flocculation TMZ studies (e.g., Manning et al., 2017) and with the stress levels estimated
 524 at QR2. Specifically, the shear stress values have been evaluated as

$$525 \quad \tau = \rho \nu_t \frac{dV}{dz} \quad (4)$$

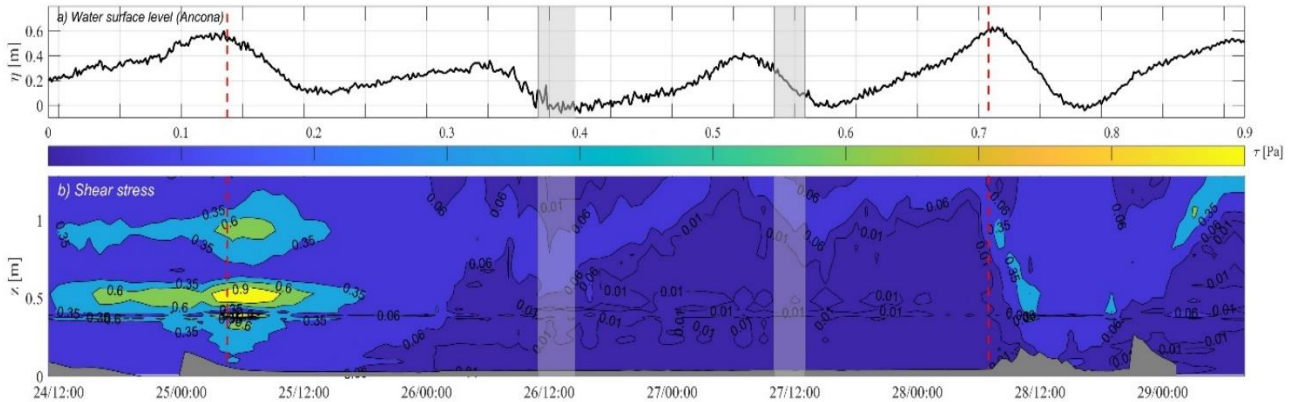
526 where V is the horizontal velocity, $\rho = 1000 \text{ kg/m}^3$ is the water density (here assumed as
 527 constant), while the eddy viscosity is defined as

$$528 \quad \nu_t = \kappa u_* z \left(1 - \frac{z}{d}\right) \quad (5)$$

529 with $\kappa = 0.41$ being the von Karman's constant and d the instantaneous water depth. The shear
 530 velocity is defined using the logarithmic velocity distribution (e.g., Bagherimiyab & Lemmin,
 531 2013):

$$532 \quad \frac{V}{u_*} = \frac{1}{\kappa} \ln \left(\frac{z}{z_0} \right) \quad (6)$$

533 where the bed roughness is estimated as $z_0 = d_{50}/30$ and the median grain diameter in the final
 534 reach of the MR is taken as $d_{50} \sim 62.5 \mu\text{m}$, corresponding to the separation between very fine sand
 535 and silt (e.g., Brocchini et al., 2013; Baldoni et al., 2022). The result is illustrated in Figure 8b,
 536 where the whole water column is characterized by relatively small values, never exceeding 0.9 Pa
 537 during the sampling activity (shaded gray areas).



538
 539 *Figure 8 – Data referring to the BS, transition and SS periods. (a) Water surface level measured by the tide gauge (Ancona).*
 540 *(b) Computed shear stress. The bed estimated from the pencil beam sonar line scans is overlaid in grey. Shaded rectangles give*
 541 *the time during sample collection, while the red vertical lines indicate the timing of the flow peak at the MR mouth.*

542 The FM outputs for the three scenarios at each location are shown in Table 2, Table 3 and
 543 Table 4, while the complete FM outputs and run parameters related to 0.25 m above the bed (at all
 544 shear stress levels) are summarized in Appendix B.2.

545 The link between the FM findings and the TMZ structure mainly concerns the transport of
 546 fines and contaminants, as well as the floc settling and depositional effects affecting the TMZ.
 547 Such aspects are discussed in Section 4.

548

549

Table 2. FM outputs for scenario 1 (SS): floc characteristics 0.25 m above bed.

| Distance from mouth [km] | Mud [%] | Sand [%] | Turbidity [NTU] | SSC [mg/l] | $W_{S_{macro}} (0.35Pa)$ [mm/s] | $W_{S_{micro}} (0.35Pa)$ [mm/s] | SPM_{ratio} | MSF (0.35Pa) [$mg \cdot m^{-2} \cdot s^{-1}$] |
|--------------------------|---------|----------|-----------------|------------|---------------------------------|---------------------------------|---------------|---|
| -0.475 | 100 | 0 | 250 | 2500 | 3.49 | 0.93 | 7.89 | 8010 |
| -0.475 | 75 | 25 | 250 | 2500 | 4.15 | 0.97 | 2.16 | 7849 |
| +0.025 | 50 | 50 | 155 | 1550 | 2.79 | 2.24 | 0.84 | 3854 |
| +0.525 | 0 | 100 | 65 | 650 | 6.80 | 6.80 | 1.00 | 4420 |

550

Table 3. FM outputs for scenario 2 (BS): floc characteristics 0.25 m above bed.

| Distance from mouth [km] | Mud [%] | Sand [%] | Turbidity [NTU] | SSC [mg/l] | $W_{S_{macro}} (0.35Pa)$ [mm/s] | $W_{S_{micro}} (0.35Pa)$ [mm/s] | SPM_{ratio} | MSF (0.35Pa) [$mg \cdot m^{-2} \cdot s^{-1}$] |
|--------------------------|---------|----------|-----------------|------------|---------------------------------|---------------------------------|---------------|---|
| -0.475 | 100 | 0 | 130 | 1300 | 2.93 | 0.93 | 4.71 | 3351 |
| -0.475 | 75 | 25 | 130 | 1300 | 3.19 | 0.69 | 1.41 | 2795 |
| +0.025 | 50 | 50 | 80 | 800 | 2.39 | 2.10 | 0.62 | 1768 |
| +0.525 | 0 | 100 | 40 | 400 | 6.80 | 6.80 | 1.00 | 2720 |

551

Table 4. FM outputs for scenario 3 (transition): floc characteristics 0.25 m above bed.

| Distance from mouth [km] | Mud [%] | Sand [%] | Turbidity [NTU] | SSC [mg/l] | $W_{S_{macro}} (0.35Pa)$ [mm/s] | $W_{S_{micro}} (0.35Pa)$ [mm/s] | SPM_{ratio} | MSF (0.35Pa) [$mg \cdot m^{-2} \cdot s^{-1}$] |
|--------------------------|---------|----------|-----------------|------------|---------------------------------|---------------------------------|---------------|---|
| -0.475 | 100 | 0 | 100 | 1000 | 2.79 | 0.93 | 3.86 | 2403 |
| -0.475 | 75 | 25 | 100 | 1000 | 2.95 | 0.61 | 1.19 | 1884 |
| +0.025 | 50 | 50 | 65 | 650 | 2.31 | 2.07 | 0.58 | 1403 |
| +0.525 | 0 | 100 | 25 | 250 | 6.80 | 6.80 | 1.00 | 1700 |

552

553 4 Discussion

554 Net estuarine circulation in MTEs similar to the MR estuary is typically determined by an
 555 important interplay between the freshwater discharge and sea forcing. Even with low tide ranges
 556 and negligible tidal currents, tidal forcing does influence the MR estuary under all freshwater
 557 conditions, especially in the lower reach, through a low-frequency modulation of river current and
 558 sea waves. About 300 m upriver of the mouth, the sea action (wind, wave, tides) is generally larger
 559 than the freshwater forcing (river discharge), thus promoting an overall net landward flow of water
 560 from coastal sources in the lower water column during quiescent periods and small storms.
 561 Similarly, ~400 m upriver from the mouth, there is a net landward flow of seawater in the lower
 562 portion of the water column during quiescent periods, whereas freshwater flows gravitationally
 563 seaward in the upper portion of the water column. The higher tide level, the thicker the seawater-
 564 intrusion layer.

565 Small storms like those observed in this study, however, lead to an interesting interplay
 566 between sea waves and river forcing. Severe storms result in freshwater discharge overwhelming
 567 seaward forcing upriver of the mouth resulting in a homogeneous freshwater column characterized
 568 by downriver seaward flow and negligible tidal modulation. In the context of TMZ formation at
 569 the MR estuary, three different scenarios are considered: 1) the episodic moderate-flow regime

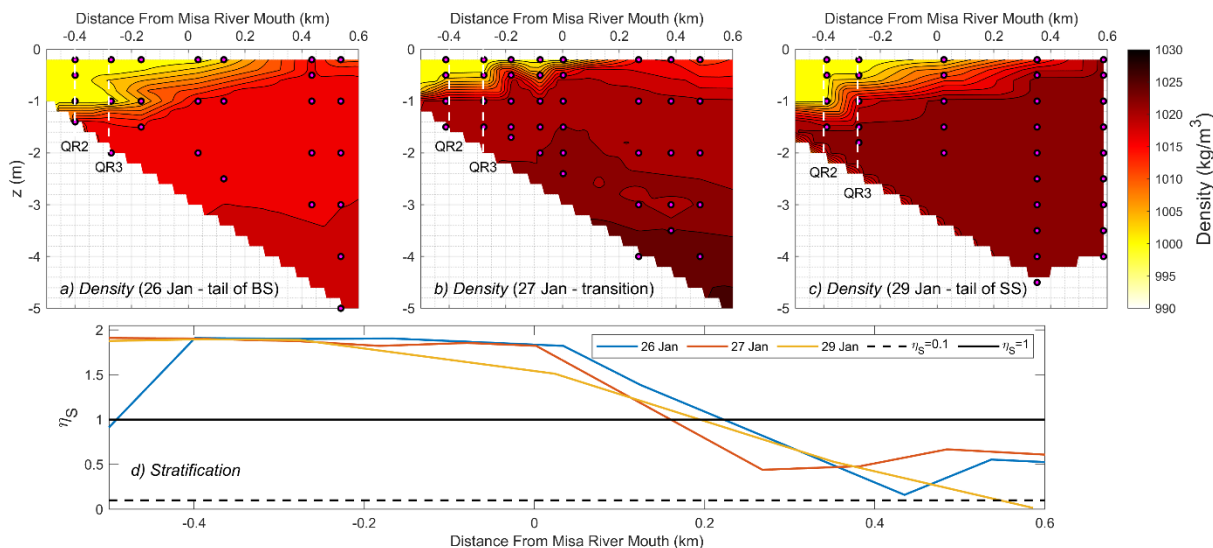
570 (represented by the SS), consisting of alternating landward-seaward flows and cross-river flows;
571 2) the episodic high-flow regime (represented by the BS), consisting of seaward flow across the
572 entire observed water column; 3) the base low-flow regime (represented by the transitional,
573 quiescent period between the BS and SS).

574 During scenario 1, both river discharge and waves at the MTE mouth are important.
575 Specifically, during the whole SS, both river flow and onshore wave energy remained nearly
576 constant at the boundaries, i.e. at Bettolle station and offshore (QS3). However, the lower river
577 flow (during the ebb tide, at low tide and in the beginning of the flood tide) facilitated the
578 propagation of low-energy/non-breaking waves into the estuary, thus leading to a strong
579 interaction between river forcing and waves at the mouth, which affected both gravitational
580 circulation and TMZ generation. In other words, the storm-induced conditions (moderate river
581 flow and increased onshore wave energy) strongly modified hydrodynamic conditions in the lower
582 reach of the MR during the SS, transitioning from a net landward-seaward flow (i.e. salt-wedge
583 behavior during lower-flow conditions) to a mainly cross-river flow (more moderate-flow
584 conditions). During this circulation regime, neither the river discharge nor onshore wave energy
585 prevailed, and significant sediment re-suspension occurred as a consequence both of the river- and
586 wave-driven fast flows and of the high shear stress that generated within the recorded water column
587 (Figure 8b). High-turbidity regions were thus generated between the two recorded sections, with
588 material being eroded and/or re-suspended at QR2 and transported downriver until flow energy
589 started to reduce in relation to onshore forcing, contributing to a large sediment deposition at QR3
590 during the ebb tide. These factors led to an ephemeral TMZ localized between QR2 and QR3, this
591 being also supported by the strong shear stress observed at QR2, which provided an increased
592 sediment transport, partially compensating the weak tidal mixing typical of MTEs and the existing
593 moderate flow condition.

594 Just after the SS, the turbidity values in the lower estuary were significantly larger than
595 those offshore. These results can be coupled with the significant salinity gradient and the well-
596 stratified structure at a distance of 300 to 600 m from the mouth, as suggested by the water density
597 (Figure 9c), which reveal a density gradient from the surface ($\sim 1,000 \text{ kg/m}^3$) to the riverbed
598 ($\sim 1,023 \text{ kg/m}^3$). Stratification significantly varied along the longitudinal transect, as shown by the
599 longitudinal distribution of η_s (yellow line, Figure 9d). The upriver/inland region was
600 characterized by a high degree of stratification level ($\eta_s > 1$), while the mid-zone region, just off
601 the MR mouth, was partially mixed ($\eta_s < 1$). Stratification further decreased from the mid-zone
602 moving toward the mouth of the MR estuary and into the offshore region ($\eta_s < 0.1$), where well-
603 mixed conditions existed. Furthermore, significant flocculation and fast macrofloc settling
604 occurred where the TMZ generates. The bio-cohesion from pure mud would have greater cohesive
605 effects and improve interparticle collision efficiency, also considering a larger macrofloc growth
606 due to the highly cohesive montmorillonite mineral (Brocchini et al., 2015). A less cohesive
607 sediment composition would provide a faster floc settling and a less efficient flocculation. The less
608 turbid and less stratified zones downriver of the TMZ were characterized by slower macroflocs
609 and quicker microflocs (lower river) or by much quicker flocs (sea), as well as much smaller MSF
610 peaks compared to those within the TMZ, but still greater than the assumption of a constant
611 0.5 mm/s . All the above results suggest that the observed TMZ during and just after the SS event
612 was a region of high flocculation and significant deposition.

613 Looking at scenario 1 in terms of a conceptual model (Figure 10a), the alternation of
614 landward-seaward flows (typical of a low-flow regime) and cross-river flows leads to high

615 turbidity near the bed at the leading edge of the seawater tongue (see the separation between green
 616 and blue shades). Cross-river flows are enhanced by the opposing river-sea forcing leading to high
 617 shear stress along the water column and resuspension of newly deposited or imported material
 618 from the lower estuary. Water column stratification and high near-bed turbidity suggest intense
 619 flocculation and large mass settling fluxes, with generation of an ephemeral TMZ downriver
 620 (seaward) of the seawater-intrusion tip (see downward arrow).

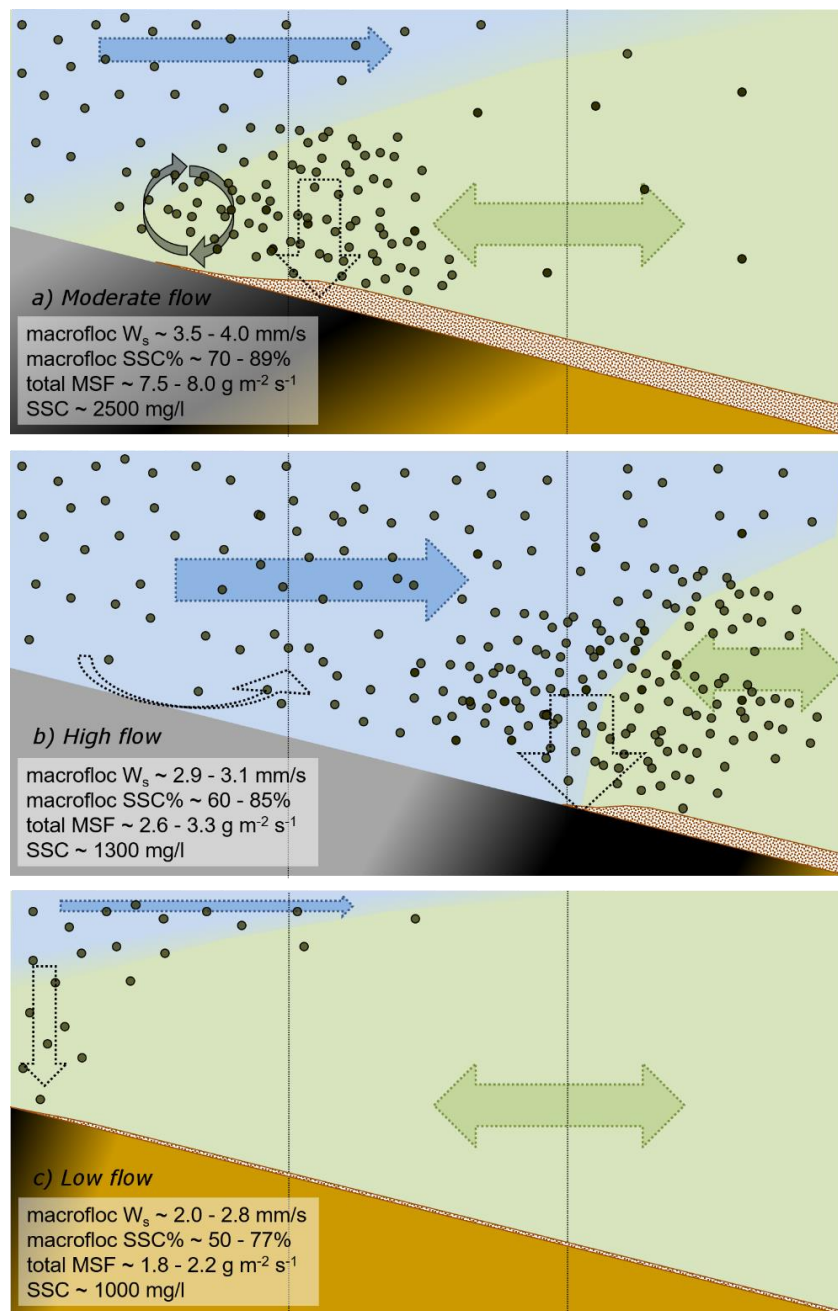


621
 622 *Figure 9 – Estimated density on: a) 26 January, b) 27 January and c) 29 January (sample locations are indicated by dots).*
 623 *d) Stratification parameter during the three sampling days.*

624 During scenario 2, estuarine circulation in the MR estuary was dominated by river
 625 discharge, with absence of the seawater-intrusion pattern and expulsion of sediments to sea. The
 626 river-discharge predominance also led to a significantly high shear stress before, during and after
 627 the storm at QR2 (Figure 8b), which was induced by the intense flow, providing a high eddy
 628 viscosity and shear velocity (see equations 4 and 5). On the other hand, the sea action was
 629 perceived far from the riverbed (e.g., at $z > 0.8$ m), where the higher intensity of the sea-induced
 630 momentum modified the directionality of the flow during the peak stage. During the end of BS,
 631 the seaward region was characterized by salinity and temperature values similar to those measured
 632 during the tail of the SS, although a different stratification regime was observed through the MR
 633 estuary (Figure 9d). Compared to what observed after the SS event, the upriver region was
 634 characterized by smaller turbidity gradients and a weaker stratification (Figure 9d). Further, the
 635 SSC at 25 cm above the bed during the tail of the BS was half of that found during the tail of the
 636 SS. Specifically, modelled floc settling dynamics were (15-20) % slower and less macrofloc mass
 637 was present. Results suggest an increase of turbulence and mixing during the BS, which led to a
 638 reduced flocculation, a slower settling and a greater particle dispersion within the water column
 639 which, in turn, promoted TMZ suppression near the riverbed (only a thin layer presents some
 640 stratification upriver of QR2, as shown in Figure 9a) during and after the BS event.

641 In a conceptual model view (Figure 10b), high-flow conditions lead to a dominance of the
 642 freshwater discharge as opposed to seaward forcing (waves and tides), resulting in well-mixed
 643 water column conditions in both river and estuary. Such conditions represent “blowout events”
 644 with mass export of suspended matter and re-suspended sediment, as testified by visual

645 observation of mats of terrestrial vegetation (Brocchini et al., 2017). The relatively low
 646 stratification leads to smaller flocs and much slower settling both around mouth and offshore (see
 647 downward arrow).



648
 649 *Figure 10 – Conceptual model representing: a) moderate-flow conditions (SS); b) high-flow conditions (BS); c) low-flow*
 650 *conditions (transition). Blue shades and arrows identify the river forcing. Green shades and arrows identify sea forcing (waves*
 651 *and tides). Black and gray arrows show the sediment-particle motion. The vertical thin lines qualitatively indicate QR2 and QR3*
 652 *locations.*

653 During scenario 3, the turbidity was significantly low in the seaward area, with the other
 654 conditions similar to those observed during the tail of the BS. However, estimated water column

655 density reached values much larger ($\sim 1026 \text{ kg/m}^3$) than those observed during the tail of both BS
656 and SS (Figure 9b), leading to a higher degree of stratification near the MR mouth (Figure 9d). In
657 the upriver region, the water column was still significantly stratified, with stratification parameters
658 similar to those observed just after the SS (Figure 9d), as also testified by the variability of the
659 shear stress along the water column, mainly induced by the vertical shear of the velocity (Figure
660 8b). A (20-25) % slowing in the floc settling velocities was observed during the transition
661 compared to what found during BS and the settling flux was typically one quarter that observed
662 during SS, with SSC being only (30-40) % of that found during SS. Typically $\text{SPM}_{\text{ratio}} < 1$, which
663 was indicative of the favoring of smaller microfloc fraction dynamics.

664 Conceptually, low-flow conditions lead to relatively high turbidity values associated with
665 the freshwater tongue of the MR in the upper water column and sea intrusion in the lower part,
666 with upriver-downriver flow separation continually modulated by the tide (Figure 10c). A
667 combination of salinity-induced flocculation and bio-cohesion potentially occurs in the final reach,
668 causing settling of fines close to the mouth and increasing their residence times within the estuary.

669

670 *4.1 Comparison with existing field studies*

671 Looking at the estuarine environments that are typically investigated worldwide, the TMZ
672 in MTEs is mainly induced by gravitational circulation and turbulence damping (e.g., Restrepo et
673 al., 2018), as supposed for the present environment. Specifically, low-flow and episodic high-flow
674 regimes in the MR promote a weakly-stratified environment, as is the case in many temperate
675 estuaries (e.g., Chesapeake Bay, Delaware Bay) characterized by moderate-to-strong tidal forcing
676 and weak-to-moderate river discharge. Conversely, episodic moderate-flow regimes in the MR
677 promote strongly stratified to salt-wedge conditions, similar to what occurs in the Columbia River
678 (e.g., Valle-Levinson, 2010). Similar behaviors have been observed in the MTE of the Neretva
679 River (eastern Adriatic Sea), characterized by tide oscillations comparable to those experienced
680 by the MR. Specifically, Krvavica et al. (2016) observed that high flow conditions weaken the
681 stratification, in contrast to typical salt-wedge estuaries, where higher river flows strengthen the
682 stratification.

683 In addition, based on a long-lasting numerical modeling, Krvavica et al. (2021) state that
684 the river inflow plays the most important role in the salt-wedge dynamics at the Neretva MTE,
685 with sea levels and tides contributing a minor effect. Although the different time scales, such
686 statement seems in contrast with what observed at the MR estuary, where the sea action is
687 fundamental for the overall estuarine dynamics during moderate-flow regimes. In particular, sea
688 waves provide significant mixing beyond tide and river flow in the lower reach of the MR, thus
689 enhancing the gravitational circulation and promoting ephemeral TMZ generation. Under these
690 conditions, as compared to higher flow conditions when the TMZ is typically located landward of
691 the seawater-intrusion tip, it generates seaward (downriver) of the seawater-intrusion tip in the MR
692 estuary. Additionally, the observed stratification is large enough to provide a significant
693 flocculation and large settling, as well as to completely suppress turbulence.

694 **5 Conclusions**

695 During storm conditions, TMZ generation was observed in the MTE of the MR. The TMZ
696 was ephemeral and was only observed during storm conditions when sea waves were impinging

697 on the mouth and the wave impact against the seaward river flow was inducing significant
698 sediment resuspension. No TMZ was present during quiescent conditions in the estuary and
699 adjacent Adriatic Sea. Consequently, differently from meso-to-hyper-tidal estuaries, the tide was
700 not a primary driver of the TMZ generation, but rather serves to modulate the overall water level
701 which in turn can affect location, intensity, and extent of ephemeral TMZs. Observations made
702 during and just after two different storms with different energy levels, show the interplay between
703 river discharge and onshore wave energy in TMZ evolution, and subsequent sediment and
704 suspended load transport in the lower reach of the MR.

705 A TMZ was present during both storms, although the vertical flow structure and its time
706 evolution were distinctly different. Specifically, the smaller storm (moderate-flow regime) was
707 associated with an interplay between river discharge and sea waves in the lower reach of the river,
708 high turbidity near the bed and significant stratification of the water column. This led to intense
709 flocculation within the estuary, fast mass settling and potential sediment transport towards the
710 mouth. On the other hand, the much greater river current observed during the bigger storm (high-
711 flow regime) produced stronger mixing, reduced the stratification, and pushed the convergence
712 area towards the mouth. Such behavior suggests that the bigger storm either pushed a mixed
713 freshwater pulse out of the mouth of the MTE (the TMZ not showing up) or suppressed the TMZ
714 near the bed by dispersing more of the suspended particulate load throughout the water column, as
715 supported by the time-evolving erosion-deposition pattern and backscatter intensity.

716 The potential for more frequent moderate-level winter storms, predicted as result of future
717 regional climatic changes exacerbated by human activities, could result in short-term (e.g., tidal
718 phase) and long-term (e.g., seasonal) impacts in the form of more regular formation of a TMZ-
719 style sedimentary flow dynamics in MTEs like those observed in the MR estuary in this study. A
720 TMZ creates an aquatic environment that is known to stimulate flocculation, and greatly alters
721 sediment settling dynamics, transport, and mass fluxes. More frequent TMZ formation in the MR
722 and in other MTEs emptying into the Adriatic Sea would result in more frequent concentrated
723 benthic suspension and fluid mud layers forming. Similar conclusions could be drawn for any
724 MTEs globally that may experience similar seasonal and episodic changes in estuarine circulation
725 in the future. The possible consequences are: longer net sedimentary particle residence time (i.e.
726 the time spent by sediments within the estuary); enhanced nearbed turbulence damping and drag
727 reduction effects; more frequent, pulsed, bulk export events; effects on nautical depth; greater
728 contaminant retention.

729

730 **Acknowledgments**

731 The financial support from the Office of Naval Research Global (UK) MORSE Project
732 (Research Grant N62909-17-1-2148) and the MIUR PRIN 2017 Project, Italy “FUNdamentals of
733 BREAKing wave-induced boundary dynamics – FUNBREAK” (Grant Number 20172B7MY9) is
734 gratefully acknowledged. AJM’s contribution towards this research was partly supported by the
735 US National Science Foundation under grants OCE-1736668 and OCE-1924532, TKI-MUSA
736 project 11204950-000-ZKS-0002, and HR Wallingford company research FineScale project
737 (ACK3013_62). J. C. was supported under base funding to the U.S. Naval Research Laboratory
738 from the Office of Naval Research. We thank our colleagues who made significant contributions
739 during the planning and execution of the field experiment including Edward F. Braithwaite III,
740 Alex Sheremet, Allen Reed, Michael Fuller, Kevin Lois. Additionally, we thank the following

741 authorities: the Municipality of Senigallia, the Capitaneria di Porto of Senigallia and of Ancona,
742 MARIDIPART La Spezia and MARIFARI Venezia. Acknowledgments go also to: GESTIPOINT
743 (Senigallia), Club Nautico (Senigallia), NOTA srl (Senigallia), Carmar Sub (Ancona), Sena
744 Gallica (Senigallia), METIS S.R.L. (Senigallia).

745

746 **References**

747 Allen, G. P., Salomon, J. C., Bassoullet, P., Du Penhoat, Y., & De Grandpre, C. (1980). Effects
748 of tides on mixing and suspended sediment transport in macrotidal estuaries. *Sedimentary*
749 *Geology*, 26(1-3), 69-90.

750 Anthony, E. J. (2015). Wave influence in the construction, shaping and destruction of river
751 deltas: A review. *Marine Geology*, 361, 53-78.

752 Bagherimiyab, F., & Lemmin, U. (2013). Shear velocity estimates in rough- bed open- channel
753 flow. *Earth surface processes and landforms*, 38(14), 1714-1724.

754 Baldoni, A., Perugini, E., Soldini, L., Calantoni, J., & Brocchini, M. (2021). Long-term evolution
755 of an inner bar at the mouth of a microtidal river. *Estuarine, Coastal and Shelf Science*,
756 262, 107573.

757 Baugh, J.V. and Manning, A.J. (2007). An Assessment of a New Settling Velocity
758 Parameterisation for Cohesive Sediment Transport Modelling. Continental Shelf
759 Research, doi:10.1016/j.csr.2007.03.003.

760 Bertin, X., & Olabarrieta, M. (2016). Relevance of infragravity waves in a wave- dominated
761 inlet. *Journal of Geophysical Research: Oceans*, 121(8), 5418-5435.

762 Best, J. L., & Leeder, M. R. (1993). Drag reduction in turbulent muddy seawater flows and some
763 sedimentary consequences. *Sedimentology*, 40(6), 1129-1137.

764 Brocchini, M. (2020). Wave- forced dynamics in the nearshore river mouths, and swash zones.
765 *Earth Surface Processes and Landforms*, 45(1), 75-95.

766 Brocchini M., Calantoni J., Reed A.H., Postacchini M., Lorenzoni C., Russo A., Mancinelli A.,
767 Corvaro S., Moriconi G., Soldini L. (2015). “Summertime conditions of a muddy
768 estuarine environment: the EsCoSed project contribution”, *Water Science & Technology*,
769 71(10), 1451-1457.

770 Brocchini, M., Calantoni, J., Postacchini, M., Sheremet, A., Staples, T., Smith, J., Reed, A.H.,
771 BraithwaiteIII, E.F., Lorenzoni, C., Russo, A., Corvaro, S., Mancinelli, A., Soldini, L.
772 (2017). Comparison between the wintertime and summertime dynamics of the Misa River
773 estuary. *Marine Geology*, 385, 27-40.

774 Burchard, H., Schuttelaars, H. M., & Ralston, D. K. (2018). Sediment trapping in estuaries.
775 *Annual review of marine science*, 10, 371-395.

776 Camuffo, D. (1984). Analysis of the series of precipitation at Padova, Italy. *Climatic Change*,
777 6(1), 57-77.

- 778 Chen, N., Krom, M. D., Wu, Y., Yu, D., & Hong, H. (2018). Storm induced estuarine turbidity
779 maxima and controls on nutrient fluxes across river-estuary-coast continuum. *Science of*
780 *the Total Environment*, 628, 1108-1120.
- 781 Colantoni, P., & Mencucci, D. (2010). Some remarks on sediment dispersion in the Central-
782 western Adriatic continental shelf. *Geology of the Adriatic Area. GeoActa*, 57-87.
- 783 Cooper, J. A. G. (2001). Geomorphological variability among microtidal estuaries from the
784 wave-dominated South African coast. *Geomorphology*, 40(1-2), 99-122.
- 785 Darvini, G., & Memmola, F. (2020). Assessment of the impact of climate variability and human
786 activities on the runoff in five catchments of the Adriatic Coast of south-central Italy.
787 *Journal of Hydrology: Regional Studies*, 31, 100712.
- 788 Davies, J. L. (1964). A morphogenic approach to world shorelines. *Zeitschrift fur*
789 *Geomorphologie*, 8, 127-142.
- 790 De Moustier, C., & Kraft, B.J. (2013). In situ beam pattern estimation from seafloor acoustic
791 backscatter measured with swath mapping sonars. *Proceedings of Meetings on Acoustics*,
792 Volume 19, Issue 1, 10.1121/1.4800560.
- 793 Dyer, K. (1986). Coastal and estuarine sediment dynamics. *John Wiley and Sons*, Chichester,
794 Sussex(UK), 1986, 358.
- 795 Dyer, K. R. (1989). Sediment processes in estuaries: future research requirements. *Journal of*
796 *Geophysical Research: Oceans*, 94(C10), 14327-14339.
- 797 Dyer, K. R., Bale, A. J., Christie, M. C., Feates, N., Jones, S., & Manning, A. J. (2002). The
798 turbidity maximum in a mesotidal estuary, the Tamar Estuary, UK: I. Dynamics of
799 suspended sediment. In *Proceedings in Marine Science* (Vol. 5, pp. 203-218). Elsevier.
- 800 Dyer, K. R., Christie, M. C., & Manning, A. J. (2004). The effects of suspended sediment on
801 turbulence within an estuarine turbidity maximum. *Estuarine, Coastal and Shelf Science*,
802 59(2), 237-248.
- 803 Eisma, D. (1986). Flocculation and de-flocculation of suspended matter in estuaries. *Netherlands*
804 *Journal of Sea Research*, 20(2-3), 183-199.
- 805 Fain, A. M. V., Ogston, A. S., & Sternberg, R. W. (2007). Sediment transport event analysis on
806 the western Adriatic continental shelf. *Continental Shelf Research*, 27(3-4), 431-451.
- 807 Favali, P., Frugoni, F., Monna, D., Rainone, M. L., Signanini, P., & Smriglio, G. (1995). The
808 1930 earthquake and the town of Senigallia (Central Italy): an approach to seismic risk
809 evaluation. *Annals of Geophysics*, 38(5-6).
- 810 Frignani, M., Langone, L., Ravaioli, M., Sorgente, D., Alvisi, F., & Albertazzi, S. (2005). Fine-
811 sediment mass balance in the western Adriatic continental shelf over a century time scale.
812 *Marine Geology*, 222, 113-133.
- 813 Geyer, W. R., Woodruff, J. D., & Traykovski, P. (2001). Sediment transport and trapping in the
814 Hudson River estuary. *Estuaries*, 24(5), 670-679.
- 815 Geyer, W. R., & MacCready, P. (2014). The estuarine circulation. *Annual review of fluid*
816 *mechanics*, 46, 175-197.

- 817 Gill, A. E. (1982). *Atmosphere-ocean dynamics* International Geophysics Series, Vol. 30,
818 Academic Press. US:California. 645 p.
- 819 Glasgow, L. A., & Luecke, R. H. (1980). Mechanisms of deaggregation for clay-polymer flocs in
820 turbulent systems. *Industrial & Engineering Chemistry Fundamentals*, 19(2), 148-156.
- 821 Gratiot, N. and Manning, A.J. (2008). Flocculation processes in concentrated benthic suspension
822 layer (CBS) using a laboratory diffusive turbulent grid tank. In: T. Kudusa, H.
823 Yamanishi, J. Spearman and J.Z. Gailani, (Eds.), *Sediment and Ecohydraulics* -Proc. In
824 Marine Science 9, Amsterdam: Elsevier, pp. 53-68, ISBN: 978-0-444-53184-1.
- 825 Hamblin, P. F. (1989). Observations and model of sediment transport near the turbidity
826 maximum of the Upper Saint Lawrence Estuary. *Journal of Geophysical Research:*
827 *Oceans*, 94(C10), 14419-14428.
- 828 Hansen, D. V., & Rattray Jr, M. (1965). Gravitational circulation in straits and estuaries. *Journal*
829 *of Marine Research*, 23, 104-122.
- 830 Horemans, D. M., Dijkstra, Y. M., Schuttelaars, H. M., Meire, P., & Cox, T. J. (2020).
831 Unraveling the essential effects of flocculation on large-scale sediment transport patterns
832 in a tide-dominated estuary. *Journal of Physical Oceanography*, 50(7), 1957-1981.
- 833 Horvath, K., Lin, Y. L., & Ivančan-Picek, B. (2008). Classification of cyclone tracks over the
834 Apennines and the Adriatic Sea. *Monthly weather review*, 136(6), 2210-2227.
- 835 Kennish, M. J. (2019). *Ecology of Estuaries: Volume 1: Physical and Chemical Aspects*. CRC
836 press.
- 837 Kirby, R., & Parker, W. R. (1982). A suspended sediment front in the Severn Estuary. *Nature*,
838 295(5848), 396-399.
- 839 Klammler, H., Penko, A. M., Staples, T., Sheremet, A., & Calantoni, J. (2021). Observations and
840 Modeling of Wave- Induced Burial and Sediment Entrainment: Likely Importance of
841 Degree of Liquefaction. *Journal of Geophysical Research: Oceans*, 126(8),
842 e2021JC017378.
- 843 Krvavica, N., Gotovac, H., & Lončar, G. (2021). Salt-wedge dynamics in microtidal Neretva
844 River estuary. *Regional Studies in Marine Science*, 43, 101713.
- 845 Krvavica, N., Travaš, V., & Ožanić, N. (2016). A field study of interfacial friction and
846 entrainment in a microtidal salt-wedge estuary. *Environmental fluid mechanics*, 16(6),
847 1223-1246.
- 848 Krone, R. B. (1963). A study of rheological properties of estuarial sediments. *Report No. 63-68*,
849 Hyd. Eng. Lab. And Sanitary Eng. Lab. University of California, Berkeley.
- 850 Lewis, R. E. (1996). Bed Generated Mixing to the Estuarine Energy Balance. *Mixing in*
851 *Estuaries and Coastal Seas*, 50, 250-266.
- 852 Li, C., & O'Donnell, J. (2005). The effect of channel length on the residual circulation in tidally
853 dominated channels. *Journal of Physical Oceanography*, 35(10), 1826-1840.
- 854 Li, M. Z. (2000). Boundary layer dynamics and drag reduction in flows of high cohesive
855 sediment suspensions. *Sedimentology*, 47(1), 71-86.

856 Lin, J., & Kuo, A. Y. (2001). Secondary turbidity maximum in a partially mixed microtidal
857 estuary. *Estuaries*, 24(5), 707-720.

858 Liungman, O., Rydberg, L., & Göransson, C. G. (2001). Modeling and observations of deep
859 water renewal and entrainment in a Swedish sill fjord. *Journal of physical oceanography*,
860 31(12), 3401-3420.

861 Llebot, C., Rueda, F. J., Solé, J., Artigas, M. L., & Estrada, M. (2014). Hydrodynamic states in a
862 wind-driven microtidal estuary (Alfacs Bay). *Journal of sea research*, 85, 263-276.

863 Manning, A. J. (2004). Observations of the properties of flocculated cohesive sediment in three
864 western European estuaries. *Journal of Coastal Research*, SI 41, 70-81.

865 Manning, A.J. (2006). LabSFLOC – A laboratory system to determine the spectral characteristics
866 of flocculating cohesive sediments. *HR Wallingford Technical Report*, TR 156.

867 Manning, A.J. (2008). The development of algorithms to parameterize the mass settling flux of
868 flocculated estuarine sediments. In: T. Kudusa, H. Yamanishi, J. Spearman and J.Z.
869 Gailani, (Eds.), *Sediment and Ecohydraulics -Proc. In Marine Science 9*, Amsterdam:
870 Elsevier, pp. 193-210, ISBN: 978-0-444-53184-1.

871 Manning, A. J., & Bass, S. J. (2006). Variability in cohesive sediment settling fluxes:
872 Observations under different estuarine tidal conditions. *Marine Geology*, 235(1-4), 177-
873 192.

874 Manning, A. J., Bass, S. J., & Dyer, K. R. (2006). Floc properties in the turbidity maximum of a
875 mesotidal estuary during neap and spring tidal conditions. *Marine Geology*, 235(1-4),
876 193-211.

877 Manning, A.J., Baugh, J.V., Spearman, J.R., Pidduck, E.L. and Whitehouse, R.J.S. (2011). The
878 settling dynamics of flocculating mud:sand mixtures: Part 1 – Empirical algorithm
879 development. *Ocean Dynamics*, INTERCOH 2009 special issue, doi: 10.1007/s10236-
880 011-0394-7.

881 Manning, A. J., & Dyer, K. R. (2002). The use of optics for the in situ determination of
882 flocculated mud characteristics. *Journal of Optics A: Pure and Applied Optics*, 4(4), S71.

883 Manning, A.J. & Dyer, K.R. (2007). Mass settling flux of fine sediments in Northern European
884 estuaries: measurements and predictions. *Marine Geology*, 245, 107-122,
885 doi:10.1016/j.margeo.2007.07.005.

886 Manning, A. J., Langston, W. J., & Jonas, P. J. C. (2010). A review of sediment dynamics in the
887 Severn Estuary: influence of flocculation. *Marine Pollution Bulletin*, 61(1-3), 37-51.

888 Manning, A. J., Whitehouse, R. J. S., & Uncles, R. J. (2017). Suspended particulate matter: the
889 measurements of flocs. *ECSA practical handbooks on survey and analysis methods:
890 Estuarine and coastal hydrography and sedimentology*, 211-260.

891 Mehta, A. J. (2013). *An introduction to hydraulics of fine sediment transport* (Vol. 38). World
892 Scientific Publishing Company.

893 Mehta, A. J., & Lott, J. W. (1987). Sorting of fine sediment during deposition. In *Coastal
894 Sediments* (pp. 348-362). ASCE.

- 895 Mehta, A. J., Manning, A. J., & Khare, Y. P. (2014). A note on the Krone deposition equation
896 and significance of floc aggregation. *Marine Geology*, 354, 34-39.
- 897 Melito, L., Postacchini, M., Darvini, G., & Brocchini, M. (2018). Waves and Currents at a River
898 Mouth: The Role of Macrovortices, Sub-Grid Turbulence and Seabed Friction. *Water*,
899 10(5), 550.
- 900 Melito, L., Postacchini, M., Sheremet, A., Calantoni, J., Zitti, G., Darvini, G., Penna, P., &
901 Brocchini, M. (2020). Hydrodynamics at a microtidal inlet: analysis of propagation of the
902 main wave components. *Estuarine, Coastal and Shelf Science*, 106603.
- 903 Milliman, J. D., & Syvitski, J. P. (1992). Geomorphic/tectonic control of sediment discharge to
904 the ocean: the importance of small mountainous rivers. *The journal of Geology*, 100(5),
905 525-544.
- 906 Monbet, Y. (1992). Control of phytoplankton biomass in estuaries: a comparative analysis of
907 microtidal and macrotidal estuaries. *Estuaries*, 15(4), 563-571.
- 908 Niedda, M., & Greppi, M. (2007). Tidal, seiche and wind dynamics in a small lagoon in the
909 Mediterranean Sea. *Estuarine, Coastal and Shelf Science*, 74(1-2), 21-30.
- 910 Nunes-Vaz, R. A., Lennon, G. W., & Bowers, D. G. (1990). Physical behaviour of a large,
911 negative or inverse estuary. *Continental Shelf Research*, 10(3), 277-304.
- 912 Orlic, M., Gacic, M., & Laviolette, P. E. (1992). The currents and circulation of the Adriatic Sea.
913 *Oceanologica acta*, 15(2), 109-124.
- 914 Pawlowicz, R., Beardsley, B., & Lentz, S. (2002). Classical tidal harmonic analysis including
915 error estimates in MATLAB using T_TIDE. *Computers & Geosciences*, 28(8), 929-937.
- 916 Postacchini, M., Melito, L., Sheremet, A., Calantoni, J., Darvini, G., Corvaro, S., ... &
917 Brocchini, M. (2020). Upstream Propagating Long-Wave Modes at a Microtidal River
918 Mouth. In *Environmental Sciences Proceedings* (Vol. 2, No. 1, p. 15). Multidisciplinary
919 Digital Publishing Institute.
- 920 Postacchini, M., Darvini, G., Perugini, E., Martinelli, J., Ilari, M., Brocchini, M. (2022). Upriver
921 Propagation of Tidal Waves and Mouth Bar Influence at a Microtidal Estuary:
922 Observations and Modeling. In *39th IAHR World Congress 2022: From snow to sea*.
923 IAHR.
- 924 Postma, H. (1980). Chemistry and biogeochemistry of estuaries.
- 925 Prandle, D. (2009). *Estuaries: dynamics, mixing, sedimentation and morphology*. Cambridge
926 University Press.
- 927 Pritchard, D. W. (1967). What is an estuary: physical viewpoint. American Association for the
928 Advancement of Science.
- 929 Restrepo, J. C., Schrottke, K., Traini, C., Bartholomae, A., Ospino, S., Ortíz, J. C., ... &
930 Orejarena, A. (2018). Estuarine and sediment dynamics in a microtidal tropical estuary of
931 high fluvial discharge: Magdalena River (Colombia, South America). *Marine Geology*,
932 398, 86-98.
- 933 Ross, M. A., & Mehta, A. J. (1989). On the mechanics of lutoclines and fluid mud. *Journal of*
934 *Coastal Research*, 51-62.

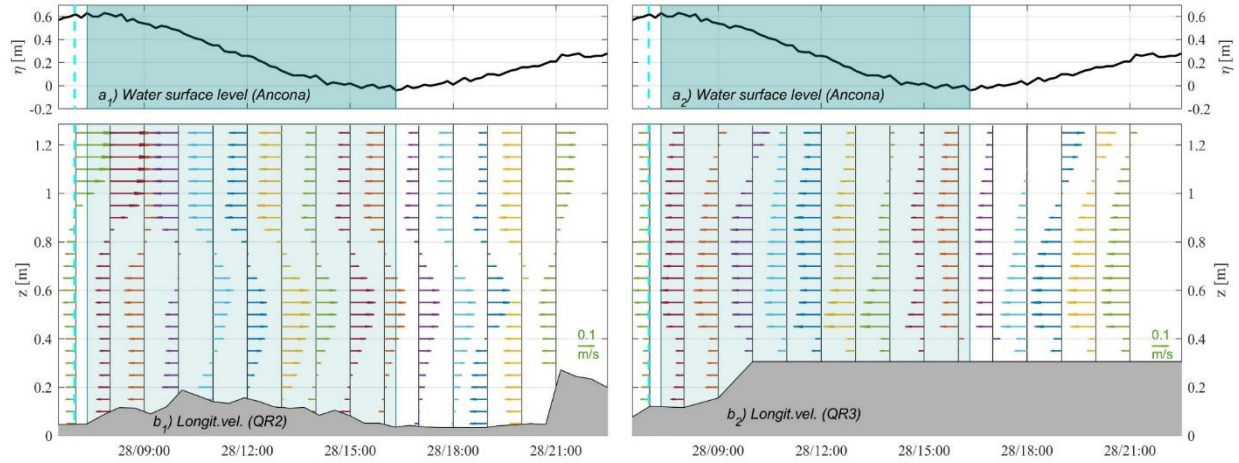
- 935 Schubel, J. R. (1968). Turbidity maximum of the northern Chesapeake Bay. *Science*, 161(3845),
936 1013-1015.
- 937 Soldini, L., & Darvini, G. (2017). Extreme rainfall statistics in the Marche region, Italy.
938 *Hydrology Research*, 48(3), 686-700.
- 939 Soulsby, R.L., Manning, A.J., Spearman, J. and Whitehouse, R.J.S. (2013). Settling velocity and
940 mass settling flux of flocculated estuarine sediments. *Marine Geology*,
941 doi.org/10.1016/j.margeo.2013.04.006.
- 942 Souto, C., Gilcoto, M., Fariña- Busto, L., & Pérez, F. F. (2003). Modeling the residual
943 circulation of a coastal embayment affected by wind- driven upwelling: Circulation of
944 the Ría de Vigo (NW Spain). *Journal of Geophysical Research: Oceans*, 108(C11).
- 945 Spearman, J. and Manning, A.J. (2008). On the significance of mud transport algorithms for the
946 modelling of intertidal flats. In: T. Kudusa, H. Yamanishi, J. Spearman and J.Z. Gailani,
947 (Eds.), *Sediment and Ecohydraulics - Proc. in Marine Science 9*, Amsterdam: Elsevier,
948 pp. 411-430, ISBN: 978-0-444-53184-1.
- 949 Spearman, J.R., Manning, A.J. and Whitehouse, R.J.S. (2011). The settling dynamics of
950 flocculating mud:sand mixtures: Part 2 – Numerical modelling. *Ocean Dynamics*,
951 INTERCOH 2009 special issue, doi: 10.1007/s10236-011-0385-8.
- 952 Spencer, K.L., Manning, A.J., Droppo, I.G., Leppard, G.G. and Benson, T. (2010). Dynamic
953 interactions between cohesive sediment tracers and natural mud. *Journal of Soils and*
954 *Sediments*, Volume 10 (7), doi:10.1007/s11368-010-0291-6.
- 955 Stommel, H., & Farmer, H. G. (1953). Control of salinity in an estuary by a transition. *J. Mar.*
956 *Res*, 12(1), 13-20.
- 957 Talke, S. A., de Swart, H. E., & De Jonge, V. N. (2009). An idealized model and systematic
958 process study of oxygen depletion in highly turbid estuaries. *Estuaries and coasts*, 32(4),
959 602-620.
- 960 Tambo, N., & Watanabe, Y. (1979). Physical characteristics of flocs—I. The floc density
961 function and aluminium floc. *Water Research*, 13(5), 409-419.
- 962 Tomadin, L. (2000). Sedimentary fluxes and different dispersion mechanisms of the clay
963 sediments in the Adriatic Basin. *Rendiconti Lincei*, 11(3), 161-174.
- 964 Uncles, R. J., Elliott, R. C. A., & Weston, S. A. (1985). Observed fluxes of water, salt and
965 suspended sediment in a partly mixed estuary. *Estuarine, Coastal and Shelf Science*,
966 20(2), 147-167.
- 967 Uncles, R. J., Joint, I., & Stephens, J. A. (1998). Transport and retention of suspended particulate
968 matter and bacteria in the Humber-Ouse Estuary, United Kingdom, and their relationship
969 to hypoxia and anoxia. *Estuaries*, 21(4), 597-612.
- 970 Uncles, R. J., Stephens, J. A., & Smith, R. E. (2002). The dependence of estuarine turbidity on
971 tidal intrusion length, tidal range and residence time. *Continental Shelf Research*, 22(11-
972 13), 1835-1856.
- 973 Valle-Levinson, A. (Ed.). (2010). *Contemporary issues in estuarine physics*. Cambridge
974 University Press.

- 975 Whitehouse, R.J.S. and Manning, A.J. (2007). Mixing it: how marine mud and sand interact.
976 *Innovation and Research Focus*, Institution of Civil Engineering publishing by Thomas
977 Telford Services Ltd (London, UK), 71, pp.2.
- 978 Whitehouse, R. J. S., Soulsby, R., Roberts, W., Mitchener, H. J. (2000). Dynamics of Estuarine
979 Muds. London: Thomas Telford Publications.
- 980 Wijeratne, E. M. S., & Rydberg, L. (2007). Modelling and observations of tidal wave
981 propagation, circulation and residence times in Puttalam Lagoon, Sri Lanka. *Estuarine,*
982 *Coastal and Shelf Science*, 74(4), 697-708.
- 983 Winterwerp, J. C., & Van Kesteren, W. G. (2004). *Introduction to the physics of cohesive*
984 *sediment dynamics in the marine environment*. Elsevier.
- 985 Wolanski, E., Chappell, J., Ridd, P., & Vertessy, R. (1988). Fluidization of mud in estuaries.
986 *Journal of Geophysical Research: Oceans*, 93(C3), 2351-2361.
- 987 Zhang, N., Thompson, C.E.L., Townend, I.H., Rankin, K.E., Paterson, D.M. and Manning, A.J.
988 (2018). Nondestructive 3D Imaging and Quantification of Hydrated Biofilm-Sediment
989 Aggregates Using X- ray Microcomputed Tomography. *Environmental Science and*
990 *Technology*, 52, 13306-13313, DOI: 10.1021/acs.est.8b03997
991

992 **Appendix A: Hydrodynamic data**

993 **A.1 Longitudinal velocity during the small storm**

994 A close-up view of the vertical profile of the longitudinal velocities is illustrated in Figure
995 A. 1. The velocity profiles represent the longitudinal velocity contribution on 28/01/2014, between
996 07:00 and 21:00, with time step of one hour. It is worth noting that the sediment deposition exists
997 when the classical seawater-intrusion pattern establishes, while erosion occurs when the sea wave
998 forcing dominates over the river flow, i.e. between ~10:00 and ~20:00.

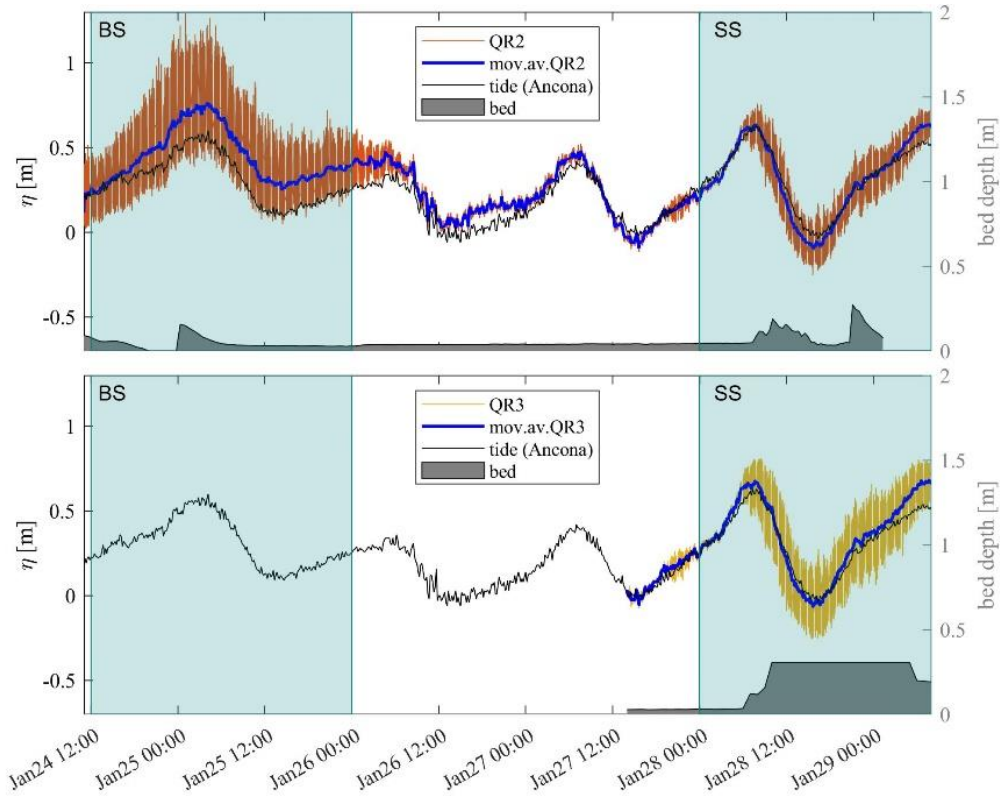


999
1000 *Figure A. 1 - Data collected during the SS. a) Water surface level at the tide gauge (Ancona). b) Longitudinal velocity component*
1001 *on 28/01/2014 (between 07:00 and 21:00, every hour). The location of the bed estimated from hourly averages of the pencil*
1002 *beam sonar line scans is overlaid in grey. Shaded areas highlight the period during which ebb tide occurred.*

1003

1004 **A.2 Analysis of water elevations at river quadpod locations**

1005 The comparison between tide-gauge signal and time-averaged water level at QR2 and QR3
1006 shows an increase of the water elevation at the MR site in the end of the SS and a negligible sinking
1007 for both quadpods (Figure A. 2), this reinforcing the theory that the material on the quadpod feet
1008 was deposited sediment and not local sediment.



1009 *Figure A. 2 – Comparison of tide-gauge signal (black lines) with instantaneous (colored lines) and time-averaged (blue lines)*
1010 *water-surface elevation at QR2 (top) and QR3 (bottom). The bed level is reported as a gray area, while shaded areas highlight*
1011 *times during which BS and SS occurred.*

1013

1014 **Appendix B: Outline of empirical Flocculation Model**

1015 ***B.1 Outline of empirical Flocculation Model***

1016 The Flocculation Model (FM) for settling velocity (W_s) utilized in this paper is based
1017 entirely on empirical observations (200+ floc population data sets) made using non-intrusive floc
1018 and turbulence data acquisition techniques representative of a wide range of typical coastal and
1019 estuarine conditions. The FM comprises a series of algorithms representative of suspensions
1020 comprising pure mud and through to various combinations of mud:sand mixtures.

1021 ***B.1.1 Floc Data for Algorithm Generation***

1022 Data comprised both in-situ field measurements and laboratory simulations.
1023 Approximately 200 individually observed floc populations were utilized spanning a wide range of
1024 suspended particulate matter (SPM) concentration and turbulence conditions within aquatic
1025 environments (laboratory generated and in-situ).

1026 The floc population size (D) and settling velocity spectra were sampled using the video-
1027 based INSSEV (Manning and Dyer, 2002) and LabSFLOC instruments (Manning, 2006; Manning
1028 et al., 2017).

1029 ***B.1.2 Algorithm Development***

1030 The FM algorithms were generated to be representative of suspensions of pure mud through
1031 to varying degrees of mixed sediment in terms of the particulate mass and dual settling velocities,
1032 both of which vary in response to shear stress and SPM concentration changes. Details of the FM
1033 algorithm derivations and preliminary testing of the floc settling algorithms are described by
1034 Manning and Dyer (2007), Manning (2008), and Manning et al. (2011).

1035 A parametric multiple regression technique was chosen to analyze the various empirical
1036 data matrices and generate statistical relationships from the experimental data. The aim was to
1037 separate the field of varying SPM concentration and τ empirical results, by curves representative
1038 of a number of parameter ranges. For the multiple regression, the following floc/aggregate
1039 characteristics were considered the most important and relevant: macrofloc settling velocity
1040 (W_{SMACRO}), microfloc settling velocity (W_{SMICRO}), total SPM concentration (SPM), percentage of
1041 SPM constituting the macrofloc portion of a floc population (SPM_{MACRO}), percentage of SPM
1042 constituting the microfloc portion of a floc population (SPM_{MICRO}), turbulent shear stress parameter
1043 derived from turbulence kinetic energy (τ).

1044 The FM algorithms are based on the segregation of flocs into macroflocs ($D > 160\mu m$) and
1045 microflocs ($D < 160\mu m$), which comprise the constituent particles of the macroflocs. This
1046 distinction permits the discrete computation of the mass settling flux (MSF) at any point in a
1047 coastal and estuarine water column. Equations are given for (Manning, 2004): i) the settling
1048 velocity of the macrofloc fraction; ii) the settling velocity of microflocs; iii) the ratio of macrofloc
1049 mass to microfloc mass in each floc population (SPM_{ratio}). These equations require the input of a
1050 turbulent shear stress (τ) and an SPM concentration.

1051

1052 **B.2 Results of the Flocculation Model**

1053 Table A.1, Table A.2 and Table A.3 summarize both input parameters and outputs of the FM (see Sections 2.3 and 3.4) relevant
 1054 to scenarios 1, 2 and 3, respectively. The illustrated data refer to an elevation of 0.25 m above the bed.

1055 *Table A.1. FM outputs for scenario 1 (SS): floc characteristics 0.25 m above bed.*

| Dist. from mouth [km] | Mud [%] | Sand [%] | Turbidity [NTU] | SSC [mg/l] | WS _{macro} (0.06Pa) [mm/s] | WS _{macro} (0.35Pa) [mm/s] | WS _{macro} (0.6Pa) [mm/s] | WS _{macro} (0.9Pa) [mm/s] | WS _{micro} (0.06Pa) [mm/s] | WS _{micro} (0.35Pa) [mm/s] | WS _{micro} (0.6Pa) [mm/s] | WS _{micro} (0.9Pa) [mm/s] | SPM _{ratio} | MSF (0.06Pa) [mg.m ⁻² s ⁻¹] | MSF (0.35Pa) [mg.m ⁻² s ⁻¹] | MSF (0.6Pa) [mg.m ⁻² s ⁻¹] | MSF (0.9Pa) [mg.m ⁻² s ⁻¹] |
|-----------------------|---------|----------|-----------------|------------|-------------------------------------|-------------------------------------|------------------------------------|------------------------------------|-------------------------------------|-------------------------------------|------------------------------------|------------------------------------|----------------------|--|--|---|---|
| -0.475 | 100 | 0 | 250 | 2500 | 2.34 | 3.49 | 2.70 | 1.96 | 0.43 | 0.93 | 0.86 | 0.69 | 7.89 | 5303 | 8010 | 6229 | 4543 |
| -0.475 | 75 | 25 | 250 | 2500 | 1.98 | 4.15 | 2.79 | 1.98 | 0.97 | 0.97 | 1.41 | 1.85 | 2.16 | 4151 | 7849 | 5887 | 4848 |
| +0.025 | 50 | 50 | 155 | 1550 | 1.22 | 2.79 | 3.11 | 1.38 | 1.17 | 2.24 | 2.51 | 2.19 | 0.84 | 1852 | 3854 | 4313 | 2824 |
| +0.525 | 0 | 100 | 65 | 650 | 6.80 | 6.80 | 6.80 | 6.80 | 6.80 | 6.80 | 6.80 | 6.80 | 1.00 | 4420 | 4420 | 4420 | 4420 |

1056 *Table A.2. FM outputs for scenario 2 (BS): floc characteristics 0.25 m above bed.*

| Dist. from mouth [km] | Mud [%] | Sand [%] | Turbidity [NTU] | SSC [mg/l] | WS _{macro} (0.06Pa) [mm/s] | WS _{macro} (0.35Pa) [mm/s] | WS _{macro} (0.6Pa) [mm/s] | WS _{macro} (0.9Pa) [mm/s] | WS _{micro} (0.06Pa) [mm/s] | WS _{micro} (0.35Pa) [mm/s] | WS _{micro} (0.6Pa) [mm/s] | WS _{micro} (0.9Pa) [mm/s] | SPM _{ratio} | MSF (0.06Pa) [mg.m ⁻² s ⁻¹] | MSF (0.35Pa) [mg.m ⁻² s ⁻¹] | MSF (0.6Pa) [mg.m ⁻² s ⁻¹] | MSF (0.9Pa) [mg.m ⁻² s ⁻¹] |
|-----------------------|---------|----------|-----------------|------------|-------------------------------------|-------------------------------------|------------------------------------|------------------------------------|-------------------------------------|-------------------------------------|------------------------------------|------------------------------------|----------------------|--|--|---|---|
| -0.475 | 100 | 0 | 130 | 1300 | 1.77 | 2.93 | 2.21 | 1.55 | 0.43 | 0.93 | 0.86 | 0.69 | 4.71 | 1996 | 3351 | 2563 | 1814 |
| -0.475 | 75 | 25 | 130 | 1300 | 1.02 | 3.19 | 1.96 | 1.28 | 0.69 | 0.69 | 1.12 | 1.55 | 1.41 | 1148 | 2795 | 2097 | 1809 |
| +0.025 | 50 | 50 | 80 | 800 | 0.83 | 2.39 | 2.55 | 1.05 | 1.03 | 2.10 | 2.38 | 2.07 | 0.62 | 763 | 1768 | 1956 | 1341 |
| +0.525 | 0 | 100 | 40 | 400 | 6.80 | 6.80 | 6.80 | 6.80 | 6.80 | 6.80 | 6.80 | 6.80 | 1.00 | 2720 | 2720 | 2720 | 2720 |

1057 *Table A.3. FM outputs for scenario 3 (transition): floc characteristics 0.25 m above bed.*

| Dist. from mouth [km] | Mud [%] | Sand [%] | Turbidity [NTU] | SSC [mg/l] | WS _{macro} (0.06Pa) [mm/s] | WS _{macro} (0.35Pa) [mm/s] | WS _{macro} (0.6Pa) [mm/s] | WS _{macro} (0.9Pa) [mm/s] | WS _{micro} (0.06Pa) [mm/s] | WS _{micro} (0.35Pa) [mm/s] | WS _{micro} (0.6Pa) [mm/s] | WS _{micro} (0.9Pa) [mm/s] | SPM _{ratio} | MSF (0.06Pa) [mg.m ⁻² s ⁻¹] | MSF (0.35Pa) [mg.m ⁻² s ⁻¹] | MSF (0.6Pa) [mg.m ⁻² s ⁻¹] | MSF (0.9Pa) [mg.m ⁻² s ⁻¹] |
|-----------------------|---------|----------|-----------------|------------|-------------------------------------|-------------------------------------|------------------------------------|------------------------------------|-------------------------------------|-------------------------------------|------------------------------------|------------------------------------|----------------------|--|--|---|---|
| -0.475 | 100 | 0 | 100 | 1000 | 1.63 | 2.79 | 2.09 | 1.44 | 0.43 | 0.93 | 0.86 | 0.69 | 3.86 | 1381 | 2403 | 1833 | 1286 |
| -0.475 | 75 | 25 | 100 | 1000 | 0.78 | 2.95 | 1.76 | 1.10 | 0.61 | 0.61 | 1.05 | 1.48 | 1.19 | 707 | 1884 | 1432 | 1273 |
| +0.025 | 50 | 50 | 65 | 650 | 0.75 | 2.31 | 2.43 | 0.98 | 1.00 | 2.07 | 2.36 | 2.05 | 0.58 | 592 | 1403 | 1550 | 1076 |
| +0.525 | 0 | 100 | 25 | 250 | 6.80 | 6.80 | 6.80 | 6.80 | 6.80 | 6.80 | 6.80 | 6.80 | 1.00 | 1700 | 1700 | 1700 | 1700 |

